REPORT NVL-0059-008

STUDY OF ELECTRONIC TRANSPORT AND BREAKDOWN IN THIN INSULATING FILMS

Walter C. Johnson
PRINCETON UNIVERSITY
Department of Electrical Engineering
and Computer Science
Princeton, New Jersey 08540
Telephone: (609) 452-4621

1 June 1978

SEMI-ANNUAL TECHNICAL REPORT NO. 5

Approved for public release; distribution unlimited.

Prepared for:

NIGHT VISION AND ELECTRO-OPTICS LABORATORIES
U. S. Army Electronics Command
Fort Belvoir, Virginia 22060

Sponsored by:

DEFENSE ADVANCED RESEARCH PROJECTS AGENCY

DARPA Order No. 3466
Program Code No. Y10
Contract DAAG53-76-C-0059
Effective Date: 17 November 1975
Expiration Date: 30 September 1979

Unclassified

SECURITY CLASSIFICATION OF THIS PAGE (When Data Entered)

REPORT DOCUMENTATION PAGE

READ INSTRUCTIONS BEFORE COMPLETING FORM

1. REPORT NUMBER (14) NVL-0059-008
2. GOVT ACCESSION NO.
3. RECIPIENT'S CATALOG NUMBER

4. TITLE (and Subtitle) (6)
STUDY OF ELECTRONIC TRANSPORT AND BREAKDOWN IN THIN INSULATING FILMS,

5. TYPE OF REPORT & PERIOD COVERED

6. PERFORMING ORG. REPORT NUMBER

7. AUTHOR(s) (10)
Walter C. Johnson
Telephone: (609) 452-4621

8. CONTRACT OR GRANT NUMBER(s) (15)
DAAG53-76-C-0059,
DARPA Order-3466

9. PERFORMING ORGANIZATION NAME AND ADDRESS
Princeton University
Department of Electrical Engineering
Princeton, New Jersey 08540

10. PROGRAM ELEMENT, PROJECT, TASK AREA & WORK UNIT NUMBERS
62912E, ARPA 3466,
Y10, 024CJ

11. CONTROLLING OFFICE NAME AND ADDRESS (11)
Defense Advanced Research Projects Agency
1400 Wilson Boulevard
Arlington, Virginia 22209

12. REPORT DATE
1 June 1978

13. NUMBER OF PAGES
79

14. MONITORING AGENCY NAME & ADDRESS (if different from Controlling Office) (12) 82p.
Night Vision & Electro-Optics Laboratories
DELNV-EO
Fort Belvoir, Virginia 22060

15. SECURITY CLASS. (of this report)
Unclassified

15a. DECLASSIFICATION/DOWNGRADING SCHEDULE

16. DISTRIBUTION STATEMENT (of this Report)
Approved for public release; distribution unlimited

(9) Semi-annual technical rept. no. 5,

17. DISTRIBUTION STATEMENT (of the abstract entered in Block 20, if different from Report)

18. SUPPLEMENTARY NOTES

19. KEY WORDS (Continue on reverse side if necessary and identify by block number)
Insulating Films
Electronic Transport in Insulators
Charge Trapping in Insulators
Dielectric Breakdown
Silicon Dioxide
Silicon nitride
Aluminum oxide

20. ABSTRACT (Continue on reverse side if necessary and identify by block number)
Recent progress is reported in an ongoing program of studies of high-field effects in thin insulating films on semiconducting substrates. The investigations reported here include further studies of the high-field generation of interface states and electron traps in the Si-SiO_2 system, a preliminary investigation of silicon dioxide grown at high pressure, and studies of CVD silicon nitride and aluminum oxide under high-field conditions.

79 04 03 014

DD FORM 1 JAN 73 1473 EDITION OF 1 NOV 65 IS OBSOLETE
S/N 0102-014-6601

Unclassified
SECURITY CLASSIFICATION OF THIS PAGE (When Data Entered)

400 734

LB

TABLE OF CONTENTS

Page

1. INTRODUCTION

We report here on recent progress in an ongoing program of research directed toward a basic understanding of the electronic properties of thin insulating films and of the interfaces of such films with semiconductors and metals. Of particular interest are the high-field properties, including charge-carrier injection through the interfaces, electronic transport through the insulator, charge-carrier trapping and recombination at the interfaces and in the insulator, the high-field generation of interface states and trapping centers, and the mechanisms leading to dielectric breakdown. The objective of the program is to provide a rational basis for the choice of materials, processing methods and treatment of the insulating films in order to obtain the desired performance and reliability. The insulating films under study at the present time are silicon dioxide, aluminum oxide, and silicon nitride on silicon substrates. The techniques and apparatus that we have developed under this program are, moreover, immediately applicable to the study of other types of insulating films and substrates.

We have previously reported on Ching-Shi Jenq's discovery that substantial concentrations of deep electron traps are generated in thermally grown silicon dioxide under high field conditions.[18] We have already described some of the properties of these traps,[1,2] and have pointed out the possible importance of the trap-generation phenomenon in short-channel insulated-gate field-effect transistors (IGFETs) and in dual-dielectric nonvolatile memories which utilize a thin film of silicon dioxide adjacent to a silicon substrate. In Ch. 2 of this report, Dr. Jenq describes the results of a further study of the properties of both the electron traps and the interface states that are produced by high fields in the $Si-SiO_2$ system. He finds that an anneal at 160°C reduces the number of high-field-produced interface states but, in 4 hrs, does not affect the electron traps. Because his best samples had n-type substrates, he performed most of his previous studies with a voltage of positive polarity impressed on the field plate so as to keep the substrate in accumulation. He now shows, using p-substrate samples, that similar high-field effects are produced when the field plate is biased negatively with respect to the substrate. Most of the experimentation previously

reported had been performed at liquid nitrogen temperature in order to reduce possible ionic motion and to inhibit the immediate generation of interface states.[2,3] In Sec. 2.4 of the present report Dr. Jenq shows that electron traps are also produced by high-field stressing at room temperature. In Sec. 2.5 he summarizes the results of his study.

The properties of thermally grown silicon dioxide are affected markedly by the conditions of growth and by post-growth annealing. An interesting and potentially useful processing technique is to grow the oxide in high-pressure oxygen. Genda Hu of our staff has examined some of the electronic properties of samples of this type which were kindly supplied to us by Dr. Robert Zeto of the U. S. Army Electronics Research and Development Command, Fort Monmouth, N. J. Although these samples had been used by Dr. Zeto in previous tests and were not in good condition, nevertheless they showed interestingly high breakdown strength. In addition, the amount of positive charging after high field stress was unusually small, and this may have implications in regard to radiation hardness. We suggest that these matters should be pursued further using fresh samples prepared under carefully controlled conditions.

In earlier reports,[17,18] Hu H. Chao described his development of a combined corona-photoemission method for investigating the electronic properties of thin insulating films. His technique retains the advantages of the original corona method, in which ions extracted from a corona discharge are used to charge the unmetallized surface of the insulator and thus supply the required electric field. Inherent in the original corona method was the reliance on high-field emission from the electrodes to supply the charge carriers. Dr. Chao has added a new degree of freedom into the experimentation by utilizing internal photoemission to provide the carriers, thus divorcing the mechanisms of injection and transport from each other. In the earlier reports, Dr. Chao described the results that he obtained with this method on thermally grown silicon dioxide, and in the present report he gives his results obtained on silicon nitride.

S. S. Li's work on high field effects in aluminum oxide have also been reported previously,[1,2,17] and in the present report he describes recently obtained results on the Al_2O_3-Si system. By reducing the temperature he suppressed the thermally activated component of injected current and studied the tunneling component. He has also studied a pre-breakdown instability and the breakdown itself. He finds that once the instability has manifested itself in the form of small spikes of current, the ability of the insulator to withstand high electric fields is permanently reduced, and the application of even a lower voltage will eventually lead to breakdown, perhaps many hours later. The studies are continuing, and various models of the high-field behavior of this system are being evaluated.

2. FURTHER STUDY OF HIGH FIELD EFFECTS IN MOS CAPACITORS

(Ching-Shi Jenq collaborating)

2.1. Introduction

We have reported previously[1,2] on the high-field generation of interface states and electron traps in the metal-silicon dioxide-silicon system and also on several properties of the interface states and electron traps. In Sec. 2.2 of this report we describe the effect of annealing at 160°C on the high-field-produced interface states and electron traps. In our previously described studies of the electron traps we used positive gate stress exclusively, as is explained in Sec. 2.3. In Sec. 2.3 we show the results of negative gate stress. Throughout our study of high-field effects we have chosen to stress the samples at a temperature of 90°K. This low temperature is helpful in preventing or reducing the lateral nonuniformity which may be introduced into the sample by the stress, and it also inhibits the immediate generation of interface states.[2,3] In Sec. 2.4, we show that after a sample has been stressed at room temperature, both lateral nonuniformity and new interface states are found in the sample, and new electron traps are found in the oxide. Also shown in Sec. 2.4 are the results produced by internal photoinjection of electrons at room temperature following high-field stress at 90°K. Finally, in Sec. 2.5, a summary and concluding remarks are given concerning our observations of high-field effects in MOS capacitors.

2.2. Effects of Annealing at 160°C on the Interface States and Electron Traps Generated by High-Field Stress

We have reported earlier[1,2] that the electron traps generated by high-field stress and the trapped electrons were stable at least up to 66°C. The interface-state generation induced by high-field stress at 90°K was observed to continue slowly at 66°C (or at room temperature).[1] In this section, we will describe the effects of 160°C annealing on the interface states and the electron traps.

In Fig. 2.1, the sample was a BTL, 920Å, 3% HCl, dry oxide. Curve 1 is the original interface-state density as a function of energy below the conduction band edge, as determined by Kuhn's method.[4] The sample was then stressed with a field of 7.4 MV/cm for 30 min at 90°K and was warmed up to room temperature. The resulting interface-state density

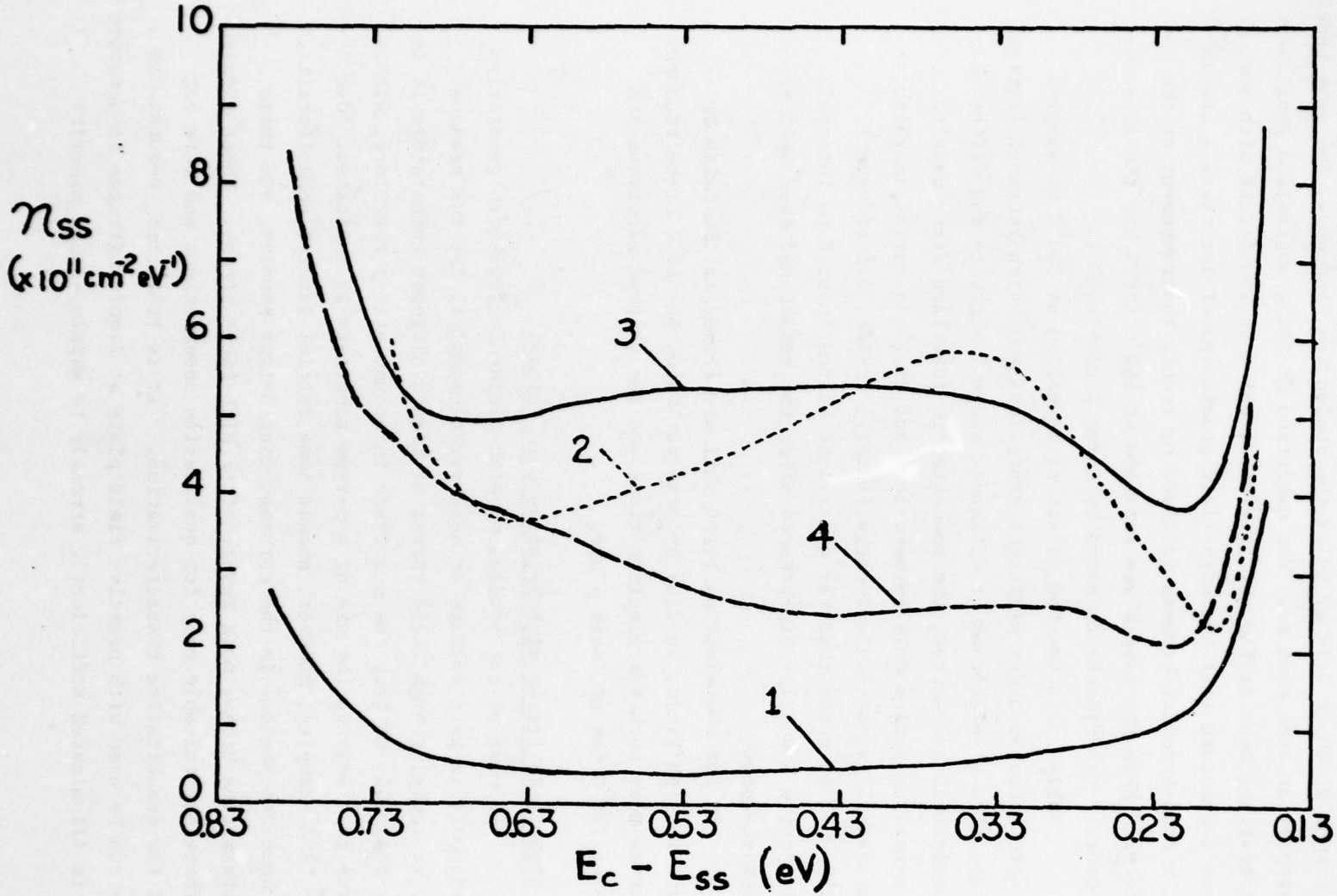

Fig. 2.1. Interface-state densities of dry-oxide MOS capacitor. Curve 1 - Before high-field stress. Curve 2 - After 7.4 MV/cm stress for 30 min. at 90°K, followed by 20-min. warmup to 66°C. Curve 3 - After 225 days at room temperature. Curve 4 - After anneal at 160°C for 4 hr.

is shown by Curve 2. Curve 3 was obtained after the sample had been held at room temperature for 225 days. Although the interface-state density measured immediately after the sample had been warmed up to room temperature shows a peak at about 0.35 eV below the conduction band edge, the peak tends to disappear as time goes on. The evolution in shape suggests a possible atomic rearrangement at SiO_2-Si interface, which is consistent with our previous conjecture that the high-field generation of interface state is due to a bond-breaking process followed by atomic rearrangement at the interface.[1] When the sample was annealed at 160°C for 4 hr, the interface state density was reduced as shown by Curve 4 of Fig. 2.1.

Table 2.1 shows the effect of annealing at 160°C on samples which were stressed under different conditions and which received internal photoinjection of electrons at different stages. Despite the differences in experimental procedures, the reduction in interface state density after annealing varies only between 16.5 and 28.2%; a variation which we can not regard as particularly significant. In Sec. 2.5 of Report NVL-0059-007[2] we noted that the donor-like states induced by internal photoinjection gradually disappeared after the sample had been held at room temperature.

As for the electron traps that are formed in the oxide by exposure to high field, we find by observation of the 66°C high-frequency C-V curves that both the electron traps and the trapped electrons are stable at 160°C for at least 4 hrs.

2.3. High-Field Stress with Negative Gate Voltage

In most of our studies of high-field electron-trap generation we used positive gate voltage on n-substrate samples, for two reasons. First, in applying high field stress at liquid nitrogen temperature it is highly desirable to keep the substrate in accumulation; therefore, with negative gate voltage the use of a p-type substrate is indicated. Our p-type (RCA) samples, however, showed some initial lateral nonuniformities which were not present in the corresponding n-type samples, and these nonuniformities became more severe after high-field stress. These samples were therefore suitable only for qualitative observations and were not useful for quantitative characterization. It is true that n-substrate sample can be used with negative field plate at liquid nitrogen temperature if it is illuminated sufficiently strongly to supply enough minority

Experimental Procedures	Stress Field and Time. (Sample No.)	N_{ss} (cm^{-2}) at the end of the last experimental step	Time (days) between the last experimental step and the thermal annealing	N_{ss} (cm^{-2}) before thermal annealing	N_{ss} (cm^{-2}) after thermal annealing (160°C for 4 hr)	% reduction in N_{ss} by thermal annealing
1. High-Field Stress at 90°k 2. Warmup	7.4 MV/cm, 60 min (BTL 7311)	3.24×10^{11}	75	3.58×10^{11}	2.88×10^{11}	19.7
	7.4 MV/cm, 30 min (BTL 3081)	2.62×10^{11}	225	3.18×10^{11}	2.28×10^{11}	28.2
1. High-Field Stress at 90°k 2. e-inj at 90°k 3. Warmup	7.4 MV/cm, 30 min (BTL3091)	1.20×10^{11}	222	1.26×10^{11}	1.05×10^{11}	16.5
1. High-Field Stress at 90°k 2. Warm up 3. e-inj at 90°k 4. Warm up	7.3 MV/cm, 30 min (RCA 5061)	3.29×10^{11} (at the end of step 2) 3.82×10^{11} (at the end of step 4)	160	3.50×10^{11}	2.80×10^{11}	19.9
1. High-Field Stress at 90°k 2. Warmup 3. e-inj at 66°C	7.3 MV/cm, 30 min (RCA 4200)	4.19×10^{11}	180	4.34×10^{11}	3.30×10^{11}	24.0

Table 2.1. Effects of annealing at 160°C for 4 hr on the reduction of interface states in samples subjected to different experimental procedures.

carriers to keep the substrate from going into deep depletion. We performed some negative-gate experiments in this way, but again quantitative characterization is hazardous because it is difficult to know exactly the voltage drop across the substrate. Although our principal, quantitatively reliable experiments were performed with positive field-plate bias on n-type samples, we have also demonstrated electron-trap generation with negative bias, and typical results are described below. The method that we employed for determining interface-state densities has been variously termed the "low-temperature ledge" (LTL) and the "low-temperature C-V displacement" (LTD) method, and it employs both a down-swept deep-depletion C-V curve and an up-swept "light-assisted" C-V curve taken after temporary illumination. A description of this technique is given in Report NVL-0059-005.[1]

The results shown in Fig. 2.2 were obtained on an n-type RCA sample with 1950Å HCl-steam oxide. Curve Set 1 was the initial 90°K deep-depletion and light-assisted C-V curves. Curve Set 2 was obtained after the field plate of the sample had been biased at 142.3V for 30 min. During the stress, the sample was illuminated with low energy light ($h\nu \leq 2$ eV) to avoid deep depletion of the substrate. The field in the oxide was approximately 7.3 MV/cm. Curve Set 2 is seen to be shifted to the right of Set 1. This is believed to be due to the trapping of electrons which tunneled into the oxide from the field plate (barrier height of 3.2 eV), the trapping being performed by electron traps which were generated during the high field stressing. After this, electrons (2.1×10^{13} cm^{-2}) were internally photoinjected into the oxide with an injection field of approximately 1 MV/cm. The C-V curves taken at this stage are Set 3, which show a further rightward shift from Set 2. This indicates further electron trapping.

Experiments similar to the above were also performed on p-type RCA samples with 1950Å HCl-steam oxides and on n-type samples with 920Å dry oxides. The results in all cases were similar to those presented above.

2.4. High-Field Stress and/or Internal Photoinjection at Room Temperature

So far we have demonstrated the generation of electron traps only on samples which were high-field stressed at 90°K. In addition, any subsequent internal photoinjection of electrons was done at 90°K. In this section we will demonstrate that a similar electron trap generation

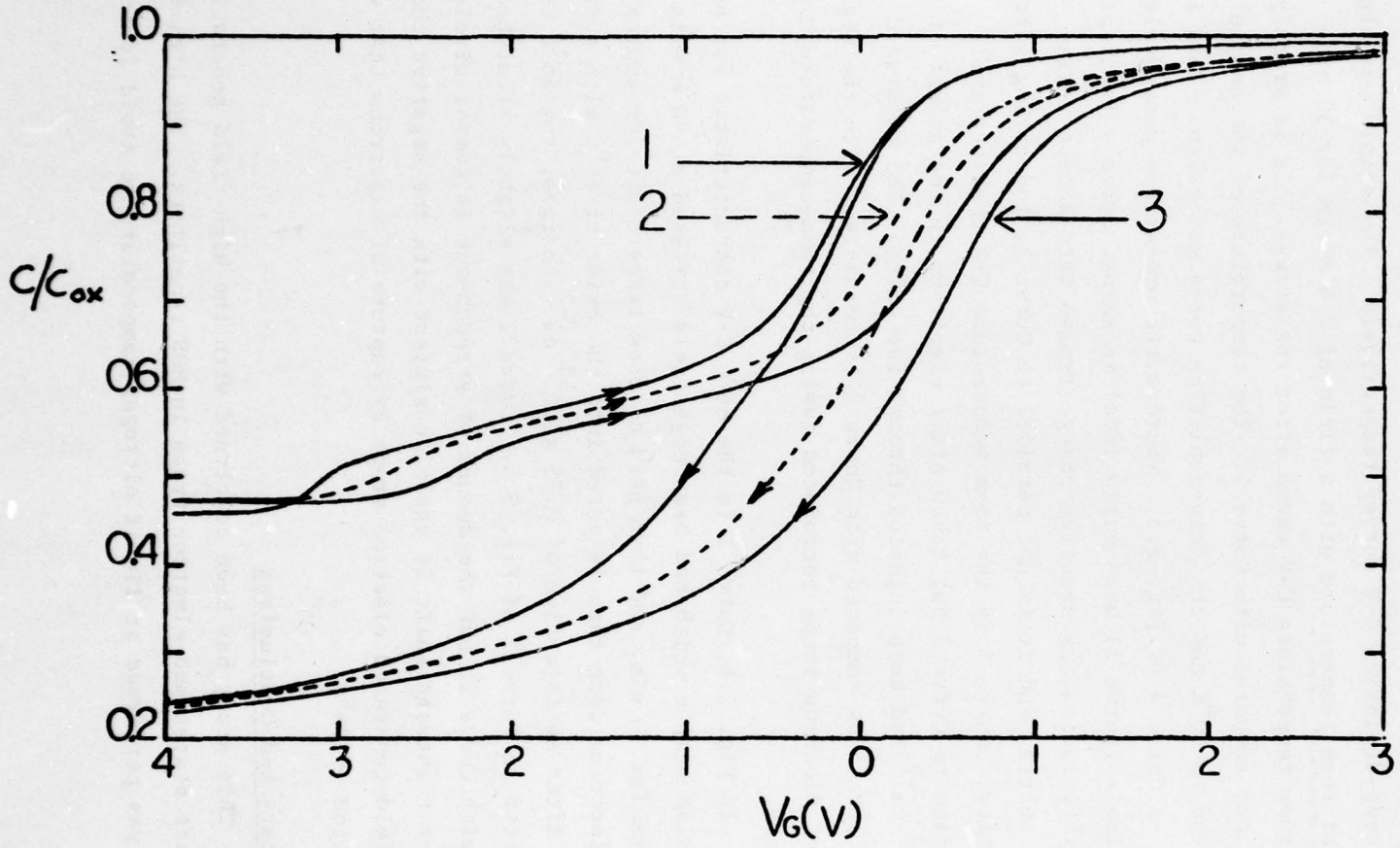

Fig. 2.2. 90°K deep-depletion and light-assisted C-V curves for an n-type RCA 1950Å oxide. Set 1: Initial condition. Set 2: After high-field stress at 90°K with a field of ∿ 7.3 MV/cm for 30 min. Set 3: After 2.1 x 10^{13} cm^{-2} electrons were injected into the oxide.

can be observed if the high-field stress is performed at room temperature. Internal photoinjection was applied either at room temperature or at 66°C to charge the electron traps.

The first example is shown in Fig. 2.3. The sample was an RCA 1950Å wet oxide. Curve 1 and Curve 2 are the initial room-temperature and 90°K deep-depletion C-V curves respectively. The sample was high-field stressed at room temperature with a field of 7.4 MV/cm for 30 min. Curve 3 is the room temperature C-V curve after the stress. It is greatly stretched out compared with Curve 1. The temperature of the sample was then reduced to 90°K and the deep-depletion curve was taken. This is presented as Curve 4 of Fig. 2.3. Whereas the pre-stress deep-depletion characteristic (Curve 2) was nearly ideal in shape, Curve 4 is displaced to the right, indicating negative charge frozen into acceptor-like interface states, and it is not parallel to Curve 2, indicating lateral nonuniformity. Curve 5 is the room temperature C-V characteristic corresponding to Curve 3 but taken after electrons in the amount of 4.1×10^{13} cm^{-2} had been injected through the oxide. The rightward shift of Curve 5 as compared with Curve 3 is consistent with the negative charging of electron traps introduced during the room-temperature high-field stress.

In Fig. 2.4, Curve 1 is the 66°C C-V characteristic for an RCA wet-oxide sample which had been high-field stressed at 90°K with a field of 7.3 MV/cm for 30 min. and then held at room temperature for approximately 34 hours. Electrons were then injected into the oxide at 66°C with a field of 1 MV/cm. After an injection of 8.75×10^{13} cm^{-2} charges, the 66°C C-V curve shifted to Curve 2 of Fig. 2.4. Curve 2 was slightly stretched out compared with Curve 1, but the amount of stretch-out is comparatively small. The rightward shift is again consistent with the negative charging of high-field-generated electron traps by capture of electrons that were photoinjected at 66°C.

2.5. Summary and Conclusions

This study has been concerned with the high-field generation of interface states and electron traps in MOS capacitors. The high-field stressing was performed at liquid nitrogen temperature to avoid ionic

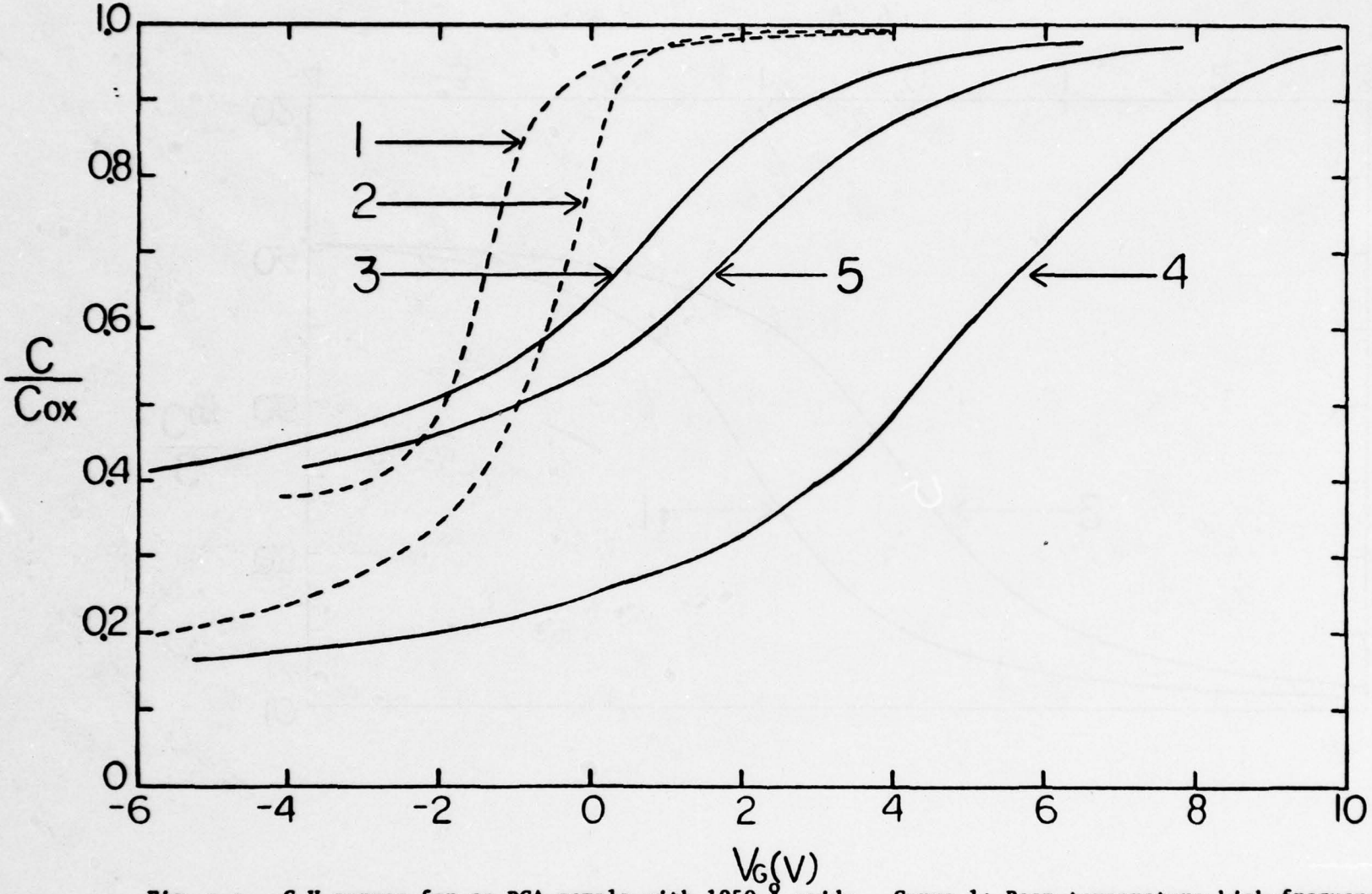

Fig. 2.3. C-V curves for an RCA sample with 1950 Å oxide. Curve 1: Room-temperature high-frequency C-V curve. Curve 2: 90°K deep-depletion curve. Curves 3 and 4: Room-temperature high-frequency and 90°K deep-depletion C-V curves after the sample had been stressed at room temperature at 7.4 MV/cm for 30 min. Curve 5: Room-temperature C-V curve after photo-injection of 4.1×10^{13} electrons/cm^2 (compare with Curve 3).

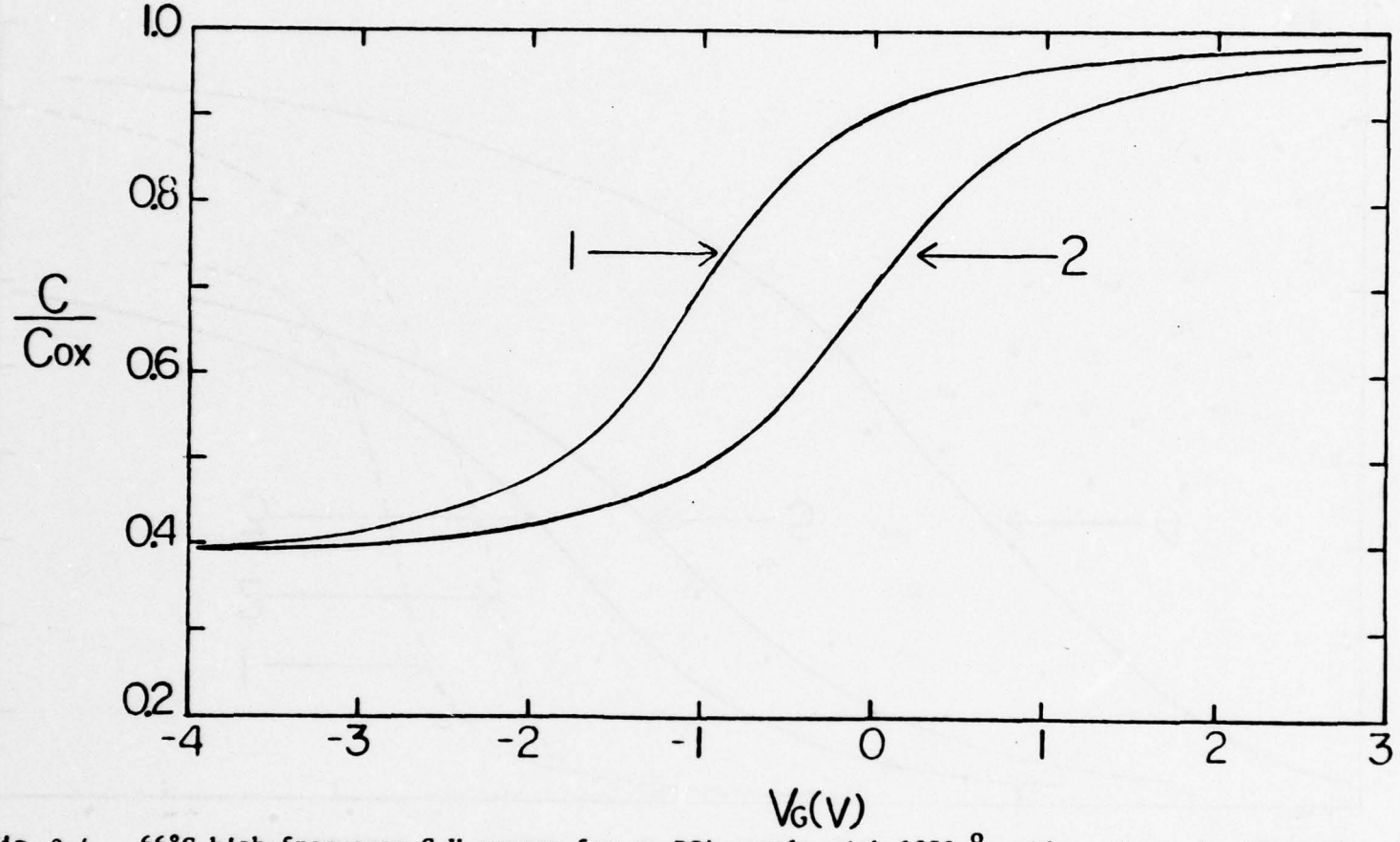

Fig. 2.4. 66°C high-frequency C-V curves for an RCA sample with 1950 Å oxide. Curve 1: After the sample was stressed at 90°K with 7.3 MV/cm for 30 min and warmed to room temperature for 34 hours. Curve 2: After 1.4×10^{-5} C/cm^2 of electrons had been internally photoinjected into the oxide at 66°C.

instability and the fast generation of interface states. A low-temperature C-V displacement method was developed to measure the interface state densities at low temperatures. Details of the procedures and results can be found in References 1, 2, and 5.

Figure 2.5 outlines the experimental procedures and summarizes the results. The MOS capacitors were first cooled to 90°K and were then stressed with high electric field. Negative charging in the oxide began to appear above a threshold field of approximately 6.8 MV/cm for both polarities of the field plate. As shown by the two branches in Fig. 2.5, experiments done with the field plate positive showed a second threshold field: 7.2 MV/cm for the BTL dry-oxide samples and 7.4 MV/cm for the RCA steam-grown oxides, at which there was a change in sign of the oxide charge observed immediately after the high-field stressing.

As shown on the left branch in Fig. 2.5, stress fields between 6.8 MV/cm and 7.2 - 7.4 MV/cm produced the following results at 90°K: (1) The oxide was found to be negatively charged immediately after stressing. (2) The interface state density remained unchanged so long as the sample was kept at 90°K. (3) Electron traps were generated in the oxide, as could be shown by the electron trapping which occurred when electrons were injected into the oxide. The post-stress negative charging of the oxide mentioned under (1) above was presumably the result of some electron capture by these traps. The thickness dependence of flatband voltage and the bias dependence of photocurrent both indicated that the traps were approximately uniformly distributed through the bulk of the oxide. As is shown on the leftmost branch in Fig. 2.5, if the sample was warmed immediately after the high-field stress, new interface states ($N_{ss(1)}$) appeared. The number of new interface states increased sharply as the stress time and stress field were increased. The electron traps were still present in the oxide after warmup. The traps were deep, as no depopulation of trapped electrons was observed upon exposure to 4 eV light. The traps and the trapped electrons were stable up to at least 160°C.

As is indicated on the second branch of the left side of Fig. 2.5, the photoinjection of electrons into the oxide before warmup produced the following results: (1) Electron traps were filled. (2) As a consequence, the net

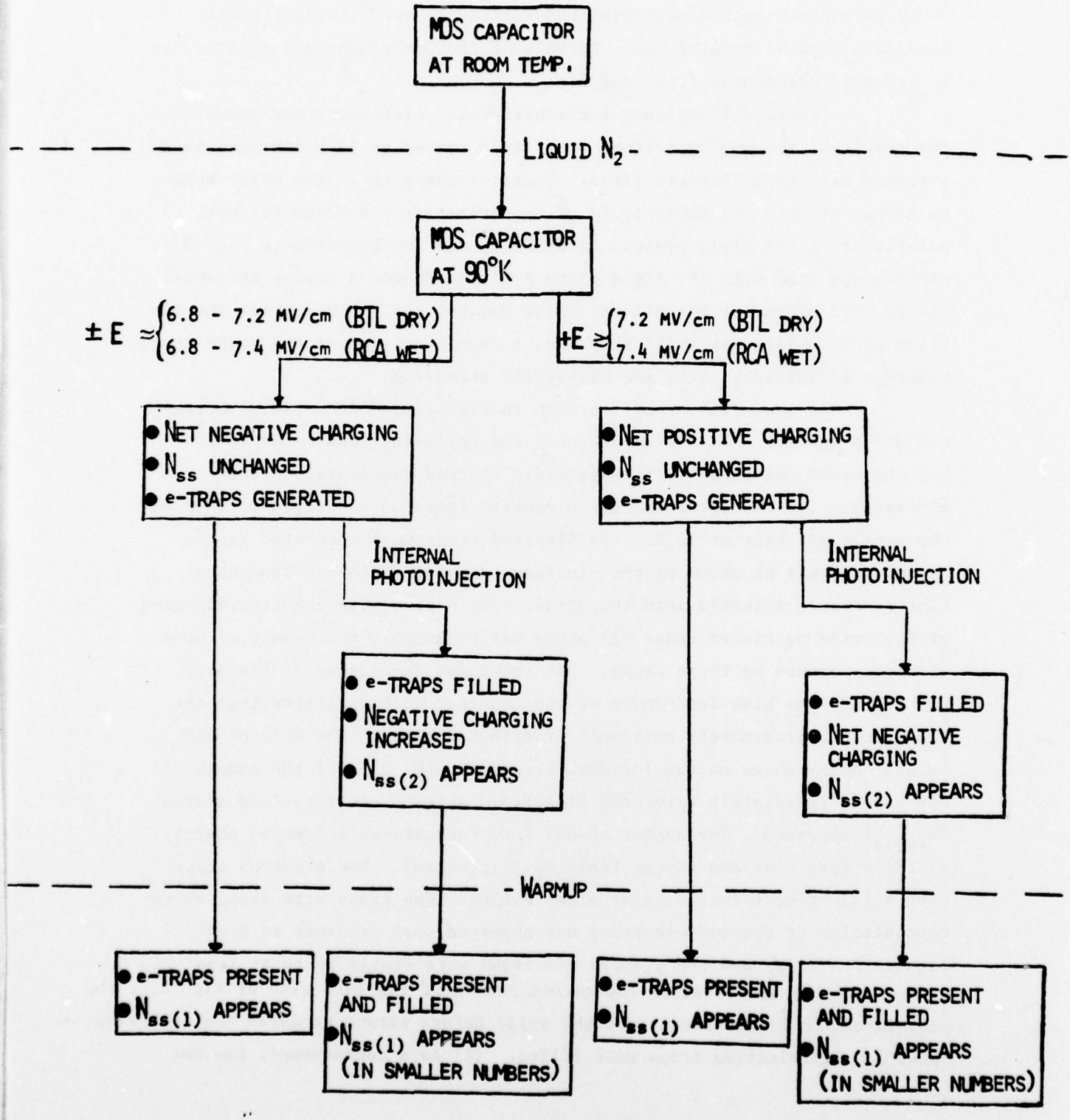

Fig. 2.5. Outline of the experimental procedures and summary of the main results. For the right two branches, experiments were done with positive field plate only (see Sec. 2.3).

negative charge in the oxide was increased. (3) Interface states ($N_{ss(2)}$), apparently of a second species as judged by the effect of temperature, appeared. If the sample was then warmed up, the electron traps were still present and filled. Interface states of species 1 ($N_{ss(1)}$) were generated, but the interface states that were induced by the internal photoinjection ($N_{ss(2)}$) began to decrease. The total number of interface states was much smaller than in those samples which had been warmed up without internal photoinjection.

As shown on the right-hand branches of Fig. 2.5, experiments performed with positive field plate at stress fields greater than 7.2 - 7.4 MV/cm produced the following results at 90°K: (1) A net positive charge was introduced into the oxide. This is believed to be due to the trapping of holes generated by impact ionization.[6] When the sample was stressed with fields of the aforementioned intensity, current multiplication was usually observed. This is an indication of the activity of impact ionization. (2) The interface state density again remained unchanged as long as the sample was at 90°K. (3) Electron traps were generated. The electron capture cross section of these were perhaps smaller than the hole capture cross section of the hole traps, which would explain why the net oxide charge was positive. If, as is shown on the next-to-last branch of Fig. 2.5, the sample was then warmed up, the electron traps were still present, and interface states of species 1 ($N_{ss(1)}$) were generated. If, as is shown on the right-hand branch of Fig. 2.5, internal photoinjection was performed before the sample was warmed up, then: (1) The electron traps became filled. (2) As a consequence, net negative charging appeared. (3) Interface states of species 2 ($N_{ss(2)}$) were induced by the electron injection. If the sample was then warmed up: (1) Electron traps were still present and filled. (2) Interface states of species 1 ($N_{ss(1)}$) were generated and $N_{ss(2)}$ began to decrease. The total number of interface states was much smaller than in those samples that had been warmed up without internal photoinjection. The difference between the two right-hand branches and the two left-hand branches is the sign of the net oxide charge immediately after high-field stressing.

The capture cross section of the electron traps was found to be about 9×10^{-14} cm^2, and was observed to be independent of the stress field and the stress time over the ranges covered in our experiments. The apparent coulombic nature of the traps, as indicated by the comparatively large cross section, together with the neutrality of the oxide before electrons were captured, may indicate that pairs of positive and negative entities were created by high-field stress and that the positive members of these pairs acted as electron traps. The generation rate of the electron traps was found to be greatly reduced under a prolonged stress time. The trap concentration appeared to increase linearly with the stress field (from 7.1 to 7.4 MV/cm).

A question that should be brought up is whether the interface-state generation and electron-trap generation are related through some common physical mechanism. A common point to both is that they occur in the same range of electric fields. An important difference is that while the traps are generated immediately at $90^{\circ}K$, the interface states do not appear until thermal energy has been supplied to activate their formation. Furthermore, a large portion of the nucleating centers can be removed, or rendered inactive, by injecting electrons through the interface at low temperature. It should be noted that these differences between electron-trap and interface-state formation should not be taken as evidence that the two are unrelated, for, as we have discussed earlier,[1] the experimental results suggest that the interface-state generation may consist of two processes: first, a bond-breaking mechanism occurring during high field stress at $90^{\circ}K$, and second, an atomic rearrangement caused by the presence of the broken bonds after the sample has been supplied with thermal energy. After the first step has been completed, the interface states are not seen because the broken bonds may have energy levels that are deeper than the valence band edge of Si so that no charge communication between the states and the Si substrate is possible. But this first step of interface state generation can also be the cause of the electron trap generation. The electron trap possibly involves a pair of centers, one positively charged and the other negatively charged. The formation of the dipole pair could be associated with the transition of an electron from a bonded state to a nearby empty state. This bond-breaking

process is proposed as the first step in interface-state generation. If, on the basis of the above argument, we assume that the mechanism responsible for the electron-trap generation is the same as the first step of interface state generation, we find no contradictory evidence except for the following point: If a stressed sample is warmed up and then cooled down, and then electrons are injected into SiO_2, the traps that capture electrons can not be depopulated by exposure to 4 eV light. The reason for this may be that the presence of the broken bonds in the SiO_2 bulk has caused a different atomic rearrangement during the warmup process than at SiO_2-Si interface so that the resulting energy levels are different, i.e., energy levels centered at 0.35 eV below the conduction band edge were created at the interface but not in the bulk. This possibility is made plausible by considering the existence of transition layers at SiO_2-Si interface.[7-12]

Another important question is whether the generation of interface states and/or electron traps is due to the electric field stress itself or to the hot electrons that exist in the oxide layer during high field stress. We have so far found it difficult to devise an effective and accurate experiment to answer this last question.

3. PRELIMINARY STUDY OF HIGH FIELD EFFECTS ON THIN FILMS OF SILICON DIOXIDE GROWN IN HIGH PRESSURE OXYGEN

(Genda Hu collaborating)

3.1. Introduction

It is well known that the electronic properties of thermally grown silicon dioxide are dependent on the methods used in oxidizing the silicon surface and in processing the film after oxidation. An interesting and potentially useful processing technique is to perform the oxidation at high pressure, either in steam or in oxygen. We report here on a preliminary study of some of the electronic properties of silicon dioxide films produced by oxidation of silicon in high-pressure oxygen. The sample was kindly supplied to us by Dr. Robert Zeto of the U. S. Army Electronics Research and Development Command, Fort Monmouth, N.J. Our sample had been prepared some months earlier and had been used extensively by Dr. Zeto in breakdown tests. As is described in Sec. 3.2, it was necessary for us to remove the old field plates ("gates") from the front surface and evaporate new ones. Owing to the age and history of the sample, and the reworking that we had to do, it is likely that the characteristics of the oxide had been degraded considerably. Nevertheless the breakdown characteristics under prolonged high-field stress were unusually good. In addition, the oxide showed comparatively little positive charging under high field stress, and this may have interesting implications with regard to radiation hardness.[13]

3.2. Samples and Experiments

The substrate was n-type (100) silicon with 1-5 Ω-cm resistivity. The oxide was grown in oxygen at 150 atm at 800°C for 2 hours, and then was annealed in nitrogen at 800°C for 1 hour. Ellipsometer measurements showed the thickness of the oxide to be 955Å. Because every one of the original field plates had been subjected to high-field breakdown, we had to etch off all the original aluminum plates and replace them. The experimental steps were as follows:

1. Upon observing the old field plates under an optical microscope (x320), we could see round smooth breakdown spots on many of the gates. This indicates that these capacitors had been broken down by high-field stress with the field plates positively biased.[6]

2. By use of a mercury probe we measured some C-V curves in the open areas between the old field plates. These curves indicated that the oxide was in satisfactory condition in these regions. We then etched off the old field plates and cleaned the surface. After this operation, the breakdown spots were not visible under the microscope.

3. New aluminum field plates were vacuum evaporated to a thickness of approximately 300Å. The area of each of the new field plates was roughly 1×10^{-3} cm^2, which was about one-tenth of the old size. The reason for using smaller field plates was to improve the chances of avoiding the previously damaged spots. About half of the newly formed capacitors were found to have good insulation.

4. In order to select the good dots, we plotted the high frequency (1 MHz) C-V curve with a Boonton 72A capacitance meter, and the quasi-static C-V characteristics by the ramp method[4] using a Keithley 610C electrometer. Both high-frequency and quasi-static C-V curves were traced by an HP 7035B X-Y recorder. A 40-mV/sec ramping rate was used for both curves. Then we cooled the sample to liquid nitrogen temperature and measured a set of low temperature curves by the Low-Temperature C-V Displacement (LTD) method.[1] From this we could obtain the density of interface states within the central portion of the silicon bandgap.

5. While maintaining the sample at liquid nitrogen temperature, a high field was applied to the sample. We started with 6 MV/cm and increased the field in 0.4V increments. Each value of field was held for one hour. At fields above 7.0 MV/cm the field increment was reduced to 0.2 MV/cm. Also, some samples were held for 15 minutes instead of one hour for each increment. The field was increased in this manner until the dot broke down. This procedure sometimes was interrupted for low temperature C-V measurements to determine the charge stored in the oxide during the high-field stress processes. Both positive and negative

field-plate biases were used in the experiment.

From the low-temperature C-V displacement tests we noticed that most of the dots showed some degree of lateral nonuniformity[14] and large quantities of interface states. Only a few dots showed good characteristics. Thus most of the dots were not suitable for quantitative analysis.

3.3. Steady-State I-V Characteristics

Figure 3.1 shows the steady state I-V characteristics plotted in the Fowler-Nordheim manner.[15] These data were taken on samples which showed negligible lateral nonuniformities. The linearity of the two lines suggests that the Fowler-Nordheim tunneling mechanism properly describes the I-V relation of the high-pressure oxide. We use the Fowler-Nordheim current equation:

$$J = \frac{e^2}{8\pi h\phi} E^2 \exp\left[-\frac{4}{3}\left(\frac{2em}{\hbar}\right)^{1/2} \phi^{3/2}/E\right]$$

where J is the current density,
E is the electric field at the injection interface,
ϕ is the barrier height in -eV,
h is the Planck constant and $\hbar = h/2\pi$,
m is the effective mass of the carrier,
e is the magnitude of the charge of an electron.

The slope of $\log(J/E^2)$ vs. $(1/E)$ plot will give us information concerning barrier height and effective mass. From the plot,

$$\text{slope (Si-)} = 2.25 \times 10^8 \text{ V/cm}$$

for positive field plate and electrons injected from the substrate, and

$$\text{slope (Al-)} = 2.07 \times 10^8 \text{ V/cm}$$

for negative field plate and electrons injected from the field plate.

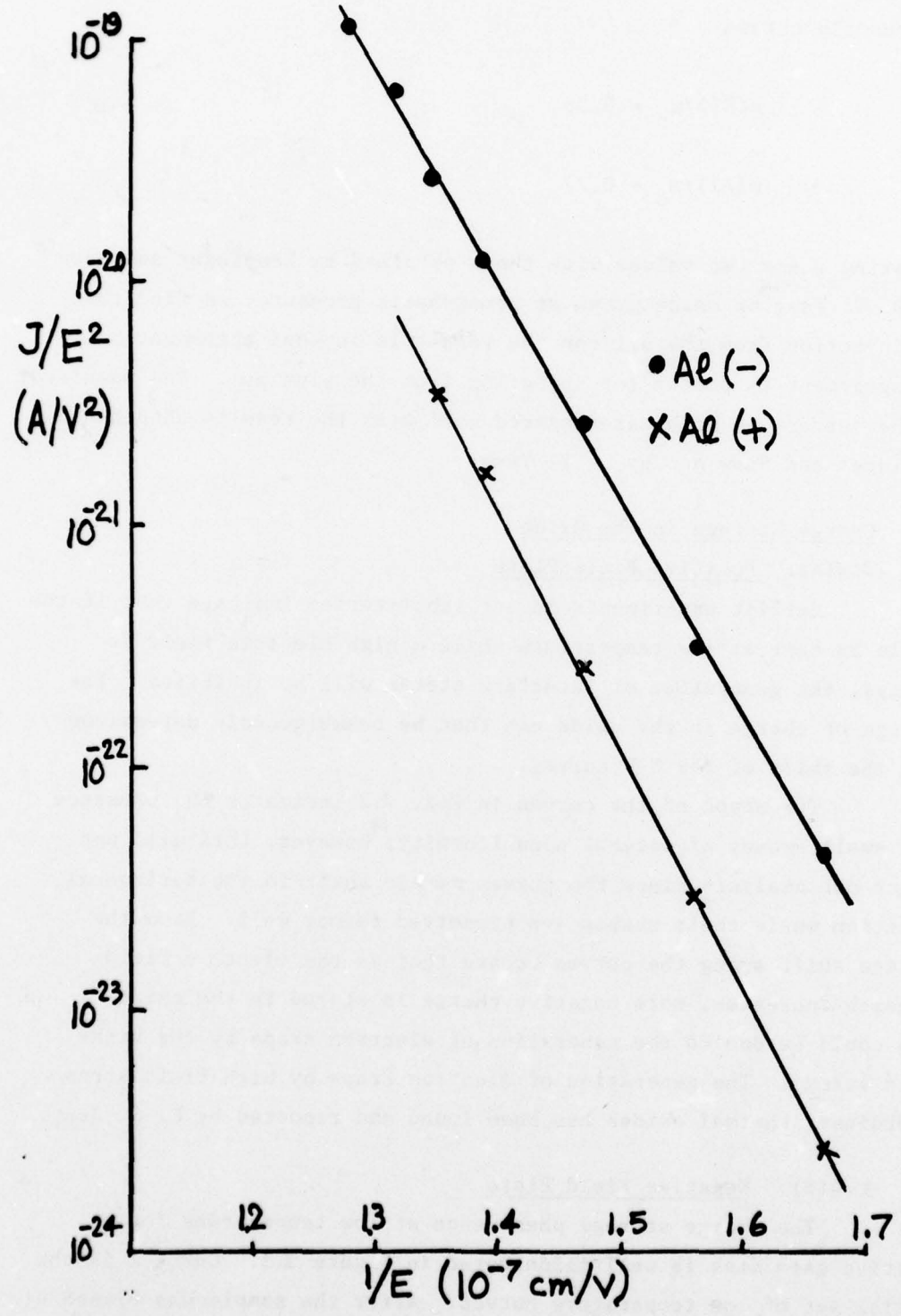

Fig. 3.1. Fowler-Nordheim plot for MOS structure with high-pressure oxide.

By using the barrier heights $\phi(Si) = 3.1$ eV and $\phi(Al) = 3.25$ eV, we may readily obtain

$$m(Si)/m_o = 0.36$$

$$m(Al)/m_o = 0.27$$

Comparing these two values with those obtained by Lenzinger and Snow[16] and D. Y. Yang[6] on oxide grown at atmospheric pressure, we find that for injection from the silicon the result is in good agreement but the agreement is poorer for injection from the aluminum. The magnitude of the current in both cases agreed well with the results obtained by Lenzinger and Snow and by D. Y. Yang.

3.4. Charge Storage in the Oxide

3.4(A). Positive Field Plate

Earlier experiments in our laboratories indicate that if the sample is kept at low temperature while a high electric field is applied, the generation of interface states will be inhibited.[1] The storage of charge in the oxide can then be unambiguously determined from the shift of the C-V curves.

The shape of the curves in Fig. 3.2 indicates the presence of a small amount of lateral nonuniformity;[14] however, this will not affect our analysis since the curves merely shift in the horizontal direction while their shapes are preserved rather well. From the voltage shift among the curves we see that as the electric field strength increases, more negative charge is stored in the oxide. This could be due to the generation of electron traps by the high-field stress. The generation of electron traps by high-field stress in ordinary thermal oxides has been found and reported by C. S. Jenq.[1,2]

3.4(B). Negative Field Plate

The charge storage phenomenon at low temperature for negative gate bias is well illustrated in Figure 3.3. Curve 1 is the initial set of low temperature curves. After the sample was biased at field of E = 7.2 MV/cm for one hour, we obtained curve 2. After

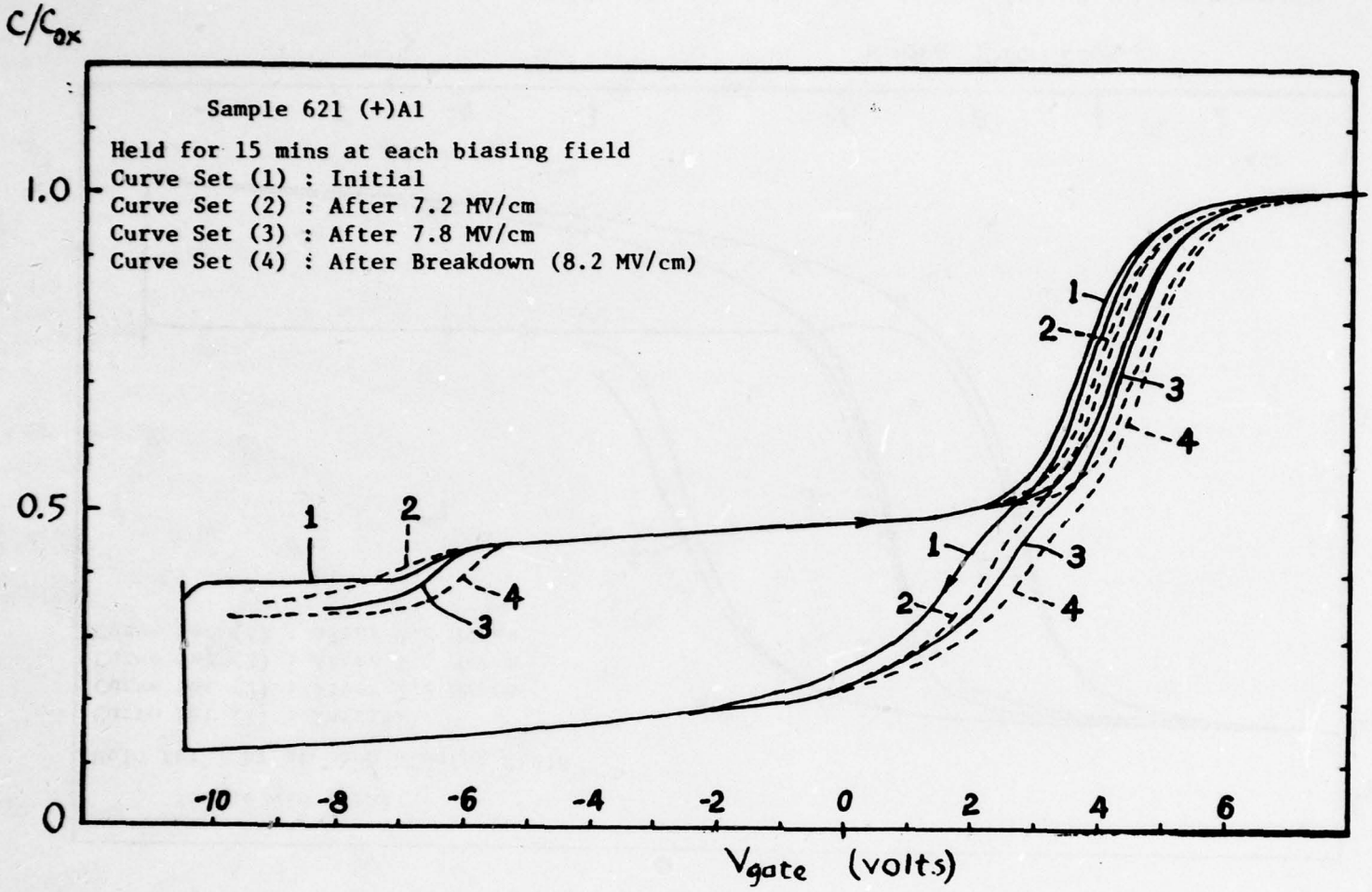

Fig. 3.2. C-V curves taken at 90°K. Set 1 - Initial condition. Set 2 - After electric field was increased to 7.2 MV/cm and held for 15 min. Set 3 - After electric field was increased to 7.8 MV/cm and held for 15 min. Set 4 - After self-quenching breakdown.

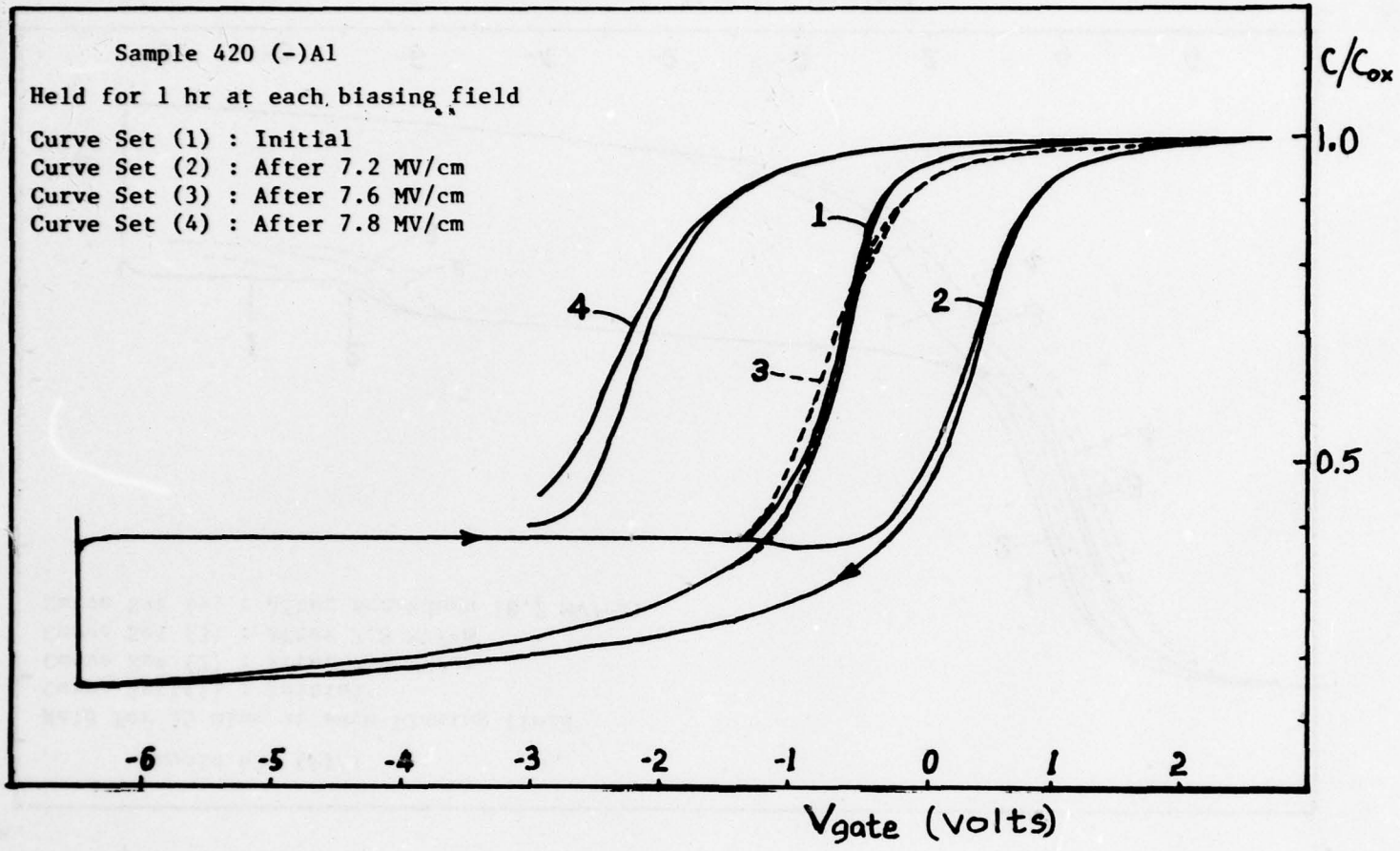

Fig. 3.3. C-V curves taken at 90°K. Set 1 - Initial condition. Set 2 - After electric field was increased to 7.2 MV/cm and held for 1 hr. Set 3 - After field was increased to 7.6 MV/cm and held for 1 hr. Set 4 - After field was increased to 7.8 MV/cm and held for 1 hr.

further bias for one hour at 7.6 MV/cm the curve moved back to approximately the initial position as shown by curve 3. Curve 4 was taken after an additional hour of bias at E = 7.8 M/cm. For $E \leq 7.2$ MV/cm, the oxide shows the same negative charge storage as it did in the positive-gate-bias case, but for E > 7.2 MV/cm there is a net storage of positive charge. This can be explained by assuming that with an n-type substrate at 900°K and negative field-plate bias, a deep depletion layer was formed in which hot holes were generated by impact ionization. Actually during the high field stress, illumination was applied in an effort to supply minority carriers so as to keep the substrate from going into deep depletion, but this effort may not have been fully effective.

3.5. Breakdown Field

Our objective in using a rather thin (300Å) field plate was to allow the self-quenching phenomenon[6] to isolate weak spots in the oxide. In determining the breakdown voltage for each dot, we used the procedure described in paragraph 5 of Sec. 3.2: While maintaining the sample at liquid-nitrogen temperature to minimize ionic motion and inhibit the generation of interface states, a voltage corresponding to an average field of 6 MV/cm was applied and held for either 15 min or one hour. The field was then increased in increments of 0.4 MV/cm, each being held for the same time as before. At 7.2 MV/cm the increments were reduced to 0.2 MV/cm. The results of these tests are shown in Table 3.1 for both polarities of applied voltage. (The breakdown listed as 8.5 MV/cm occurred as the field was being increased from 8.4 to 8.6 MV/cm.) It should be observed that the voltage at which a sample will break down depends on the amount of time allowed for conditions to stabilize. As an example of this, we were able to ramp the bias field on a sample from zero to 9.0 MV/cm without a breakdown occurring, yet if we attempted to hold this voltage for as much as 15 min, a breakdown would

Sample Number:	510	540	530	615	617	621	450
Bias time at each step:	1 hr	1 hr	15 min	1 hr	1 hr	15 min	15 min
Breakdown field (MV/cm)	8.5	8.0	8.0	7.4	7.8	8.2	7.8

(+) Al

Sample Number:	420	460	410
Bias time at each step:	1 hr	15 min	15 min
Breakdown field (MV/cm)	8.2	8.4	8.6

(-) Al

Table 3.1. List of breakdown fields for different samples at different bias conditions. Data obtained by procedure described in paragraph 5, Sec. 3.2, with each increment of field held for the time indicated.

surely occur. Our use of small increments of voltage, each being held for 15 min or one hour, was an attempt to approach the effect of a sustained voltage.

3.6. Conclusions

The observed J-E relationship for the high-pressure oxide is quite similar to that for ordinary thermal oxides, for which it has been shown that the electrical conduction is contact-limited by Fowler-Nordheim tunneling of electrons from the negative contact.[16] The absence of net positive charge in the oxide after field-plate-positive high-field stress is most interesting, for it may indicate that the high-pressure oxide has fewer hole traps near the oxide-silicon interface than ordinary thermal oxides. The net positive charging after field-plate-negative high-field stress is quite moderate. Inasmuch as hole trapping near the oxide-silicon interface is an important process contributing to radiation sensitivity of ordinary oxides,[13] we believe that the possible radiation hardness of the high-pressure oxides should be examined carefully. Finally, although our samples were in relatively poor condition, they showed unusually high values of breakdown field compared with ordinary thermal oxides, for the latter show electrical instability leading to breakdown at fields generally no greater than 7.8 MV/cm.[6] We believe that a further investigation should be conducted using fresh samples which have been prepared under carefully controlled conditions.

4. A STUDY OF SILICON NITRIDE ON SILICON BY THE COMBINED CORONA-PHOTOEMISSION TECHNIQUE

(Hu H. Chao collaborating)

4.1. Introduction

In previous reports[17,18] we have described the development of a new technique for investigating the electronic properties of thin insulating films on semiconducting substrates. This technique retains the advantages of the corona-charging method as used in the past by Williams and Willis,[19] Williams and Woods,[20] and Weinberg et al,[15] and adds the precision in charge-carrier injection afforded by internal photoinjection.[21] As in the original corona method, the surface of the insulator is left unmetallized. A corona discharge is produced in a gas at atmospheric pressure by applying a high (5-10 kV) voltage, either positive or negative, to a sharp electrode. Ions having the same polarity as the electrode are attracted to the surface of the insulator, and the resulting surface charge produces a high field in the insulating film. The almost total absence of surface conduction makes it possible to apply very high fields without the danger of destructive breakdown, and the constant-current-like character of the ionic conduction to each element of surface makes the effect of small flaws quite negligible and permits one to measure the intrinsic properties of the insulating film. The surface potential can be measured by a vibrating Kelvin probe.[15,20]

In the original corona method as described above, the field produced by the ions unfortunately serves two purposes simultaneously: it provides charge carriers by high-field injection, and it also transports these carriers through the insulator. In our combined corona-photoemission technique,[17,18,22] we use the corona ions only to provide the electric field for transport, while the carriers themselves are introduced into the insulator by means of internal photoemission, thus introducing an additional degree of freedom into the experimentation. Another important advantage of using light for the charge-carrier injection is that optical interference within the insulator can be used to maximize the excitation at either of the interfaces, thus permitting

the separation of injection effects at the two interfaces.

In our experimental work we used the combined corona-photoinjection technique to study the electronic properties of three insulator-on-silicon systems: thermally grown SiO_2 on Si, CVD Si_3N_4-thin ($\sim$ 20Å) SiO_2-Si, and CVD Si_3N_4-Si. We have reported previously on the results that we obtained on silicon dioxide,[17,18] and we shall describe here the results of our study of silicon nitride. As is well know, the composition and electronic properties of chemically vapor deposited silicon nitride depend on the processing procedures and parameters.[23-29] This point should be kept in mind when comparing the experimental results obtained by different investigators using variously prepared samples.

4.2. Sample Description

The samples were Si_3N_4-Si and Si_3N_4-SiO_2-Si structures and were supplied by RCA Laboratories. The substrates were (100) 8-10 Ω-cm n-type silicon. The backs of the wafers were doped n^+. Immediately prior to oxidation or nitride deposition, the silicon wafer was cleaned and dipped in HF solution followed by a D.I. water rinse, then dried in hot nitrogen. The thin ($\sim$ 20Å) SiO_2 layer of the Si_3N_4-SiO_2-Si sample was thermally grown in HCl-steam at 600°C. The nitride films were chemically vapor deposited at 800°C with an ammonia-to-silane ratio of 1000:1, using nitrigen as the carrier gas. Silane gas diluted to 0.5% in argon was used as the silane source. The reactor was a cold-wall quartz bell jar with an RF induction-heated silicon-coated graphite susceptor. After preparation, each wafer was sliced into square sections about 7 mm on a side.

The index of refraction and thickness of the nitride films were measured by ellipsometer* using a mercury-xenon light source. The index of refraction was 1.94 and the thickness was 1950Å ± 100 Å. An Al gate with area $.887 \times 10^{-2}$ cm^2 and thickness 5000Å was vacuum deposited on the sample. From the accumulation capacitance and the nitride thickness, the relative d.c. dielectric constant of the nitride was calculated to be 7.23. The etch rate was found to be 70Å/min in 12% HF solution.

The density of the nitride can be calculated by weighing the sample before and after the nitride etch. After the sample was weighed with a Mettler microgram balance, the back of the wafer was protected by wax and the nitride was etched off in 12% HF solution for 33 min. Then the sample was cleaned in warm trichloroethylene, acetone, and methanol and was blown dry with nitrogen. The sample was then weighed again. From the difference between the weights before and after the etching, the density of the nitride was calculated to be 2.9 gm/cm^3. A value of 3.1 gm/cm^3 is considered to be typical.

The relatively low index of refraction and high etch rate suggest that there might be some oxygen in this film.[30]

The initial flatband voltage of the Si_3N_4-Si sample was -7.6 ± 0.5 V when measured by a mercury probe. An anneal in forming gas (90% N_2, 10% H_2) at 500°C for 90 min reduced the flatband voltage to -3.5 ± 0.9 V. Alternatively, an anneal in N_2 at 500°C for 90 min reduced the flatband voltage to -2.8 ± 0.5 V. The result of etch-off experiments (using 12% HF solution) indicated that the positive charges which produced the negative flatband voltage were located at the Si-Si_3N_4 interface.

The initial flatband voltage of the Si_3N_4-SiO_2-Si sample was -5.4 ± 0.5 V. An anneal in forming gas at 500°C for 90 min reduced the flatband voltage to -4.2 ± 0.5 V. Alternatively, an anneal in nitrogen

---

* The ellipsometer measurements were performed by J. Shaw of RCA Laboratories, and we thank him for this aid.

at 500°C for 90 min reduced the flatband voltage to -1.4 ± 0.5 V. The result of etch-off experiments indicated that the positive charges were located in the thin SiO_2 layer or (within the accuracy of the determination) at one or both of its interfaces. This agrees with the result reported by Maes and Overstraeten.[31]

4.3. Light-Induced Surface Discharge after Positive or Negative Surface Charging of the Si_3N_4-Thin SiO_2-Si Structure

Before the experiments were performed, the fresh sample was annealed in either forming gas or nitrogen at 500°C for 90 min.

Positive or negative corona in dry air was used to charge the surface to the desired potential. The surface potentials used in this study correspond to average nitride fields of less than 0.6 MV/cm. After the corona was shut off, the chamber was pumped down to 10^{-3} torr. When the sample was kept in the dark, no significant change in surface potential and flatband voltage could be found after 3 hrs. Hence the charge injection into the insulator at this field can be neglected in the dark. The output of a B&L monochrometer was used to irradiate the sample for a period of time such that $|\Delta V_s| + |\Delta V_{FB}| \approx 1.5$ volts unless specified otherwise. In most cases, the flatband shift was not completely uniform over the surface of the sample: variations of as much as 20% were observed. Hence the average of the flatband voltage shifts taken at 5 different points was used. After these measurements were taken, the sample was annealed in forming gas or nitrogen at 500°C for one hour. This treatment restored the flatband voltage to within 0.1 V of its initial value and presumably brought the sample back essentially to its initial condition. After this the chamber was again filled with dry air, corona was again used to charge the surface to its former potential, the chamber was evacuated, and light with a different photon energy from before was used to discharge the sample. These processes were repeated over a range of photon energies.

The light absorption coefficient of the CVD nitride increases gradually with photon energy and there is no obvious structure which can be identified with a bandgap.[32,33] Hence, unlike thermally grown SiO_2, we cannot neglect the absorption of light having energy less than the bandgap.

Figure 4.1 shows the $(C_i|\Delta V_s|/F)^{1/2}$ vs. photon energy plot of the Si_3N_4-SiO_2-Si structure for surface potentials of 8 V and -8 V. For the negative surface potential, no change of either surface potential or flatband voltage can be observed for light with photon energy less than 4.3 eV. Therefore, for photon energies less than 4.3 eV, the absorption in the insulators, the internal photoinjection of holes from the substrate and the photoinjection of electrons from the front surface can all be neglected. This indicates that the quantum yield of hole photoinjection from the Si substrate into the insulators is very small. This is expected, for the quantum yield of hole photoinjection from the Si substrate into thermally grown SiO_2 is very small.[18]

The coincidence between the two $(C_i|\Delta V_s|/F)^{1/2}$ vs. $h\nu$ curves at large photon energies ($h\nu > 4.8$ eV) indicates that in this energy range the surface-potential discharge is due to the absorption of light in the bulk of the nitride.

With absorption, the problem becomes very complicated, making it difficult to interpret the experimental data. Hence, in the following I will concentrate on the results obtained with photon energies less than about 4.3 eV. In this energy range the optical interference model[17] can be applied.

Figure 4.2 shows a plot of $(C_i|\Delta V_s|/qTF)^{1/3}$ vs. photon energy for a surface potential of 8 V. Based on the discussion of Ch. 3 of Ref. 17, the lack of R/T structure indicates that the contribution of surface injection can be neglected. Hence the quantum yield for electron injection from Si into the insulator is

$$\text{Quantum Yield} \simeq (|\Delta V_s| + \Delta V_{FB})\, C_i/qTF$$

Figure 4.3 shows a plot of (electron injection quantum yield)$^{1/3}$ vs. photon energy for a surface potential of 8 V for the sample having 1950Å Si_3N_4 and $\sim$ 20 Å SiO_2 on Si, as was described in Sec. 4.2. This curve indicates a threshold energy of 3.7 eV. Taking into consideration Schottky barrier lowering, this corresponds to a zero-field threshold energy of 4.03 eV, which is 0.27 eV smaller than the barrier between the Si valence band and the conduction band of thermally grown SiO_2. This discrepancy can be ascribed to the thinness of the oxide and possibly also to the large

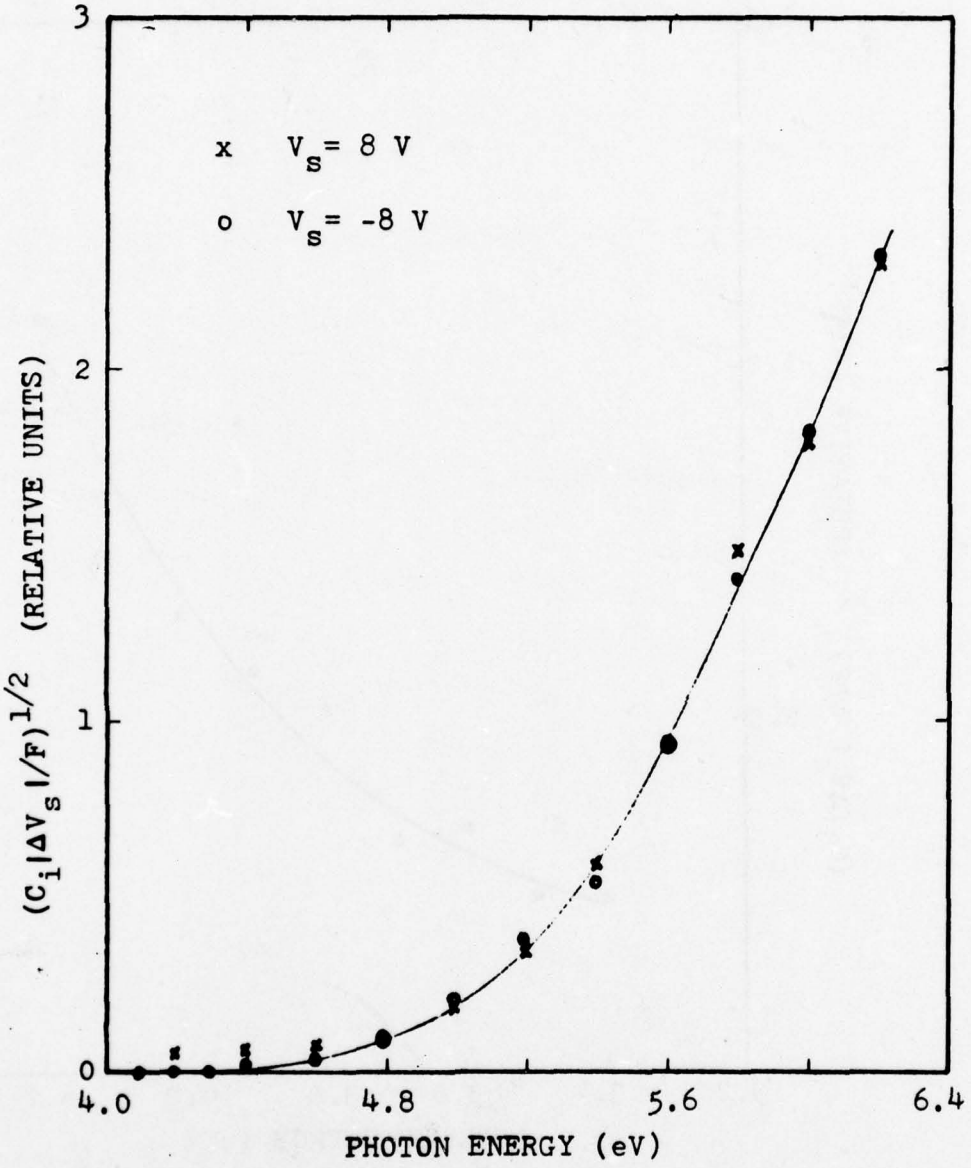

Fig. 4.1. $(C_i|\Delta V_s|/F)^{1/2}$ vs. photon energy for two surface potentials, +8 and -8V, for a structure having 1950Å Si_3N_4 and ~ 20Å SiO_2 on Si (see Sec. 4.2).

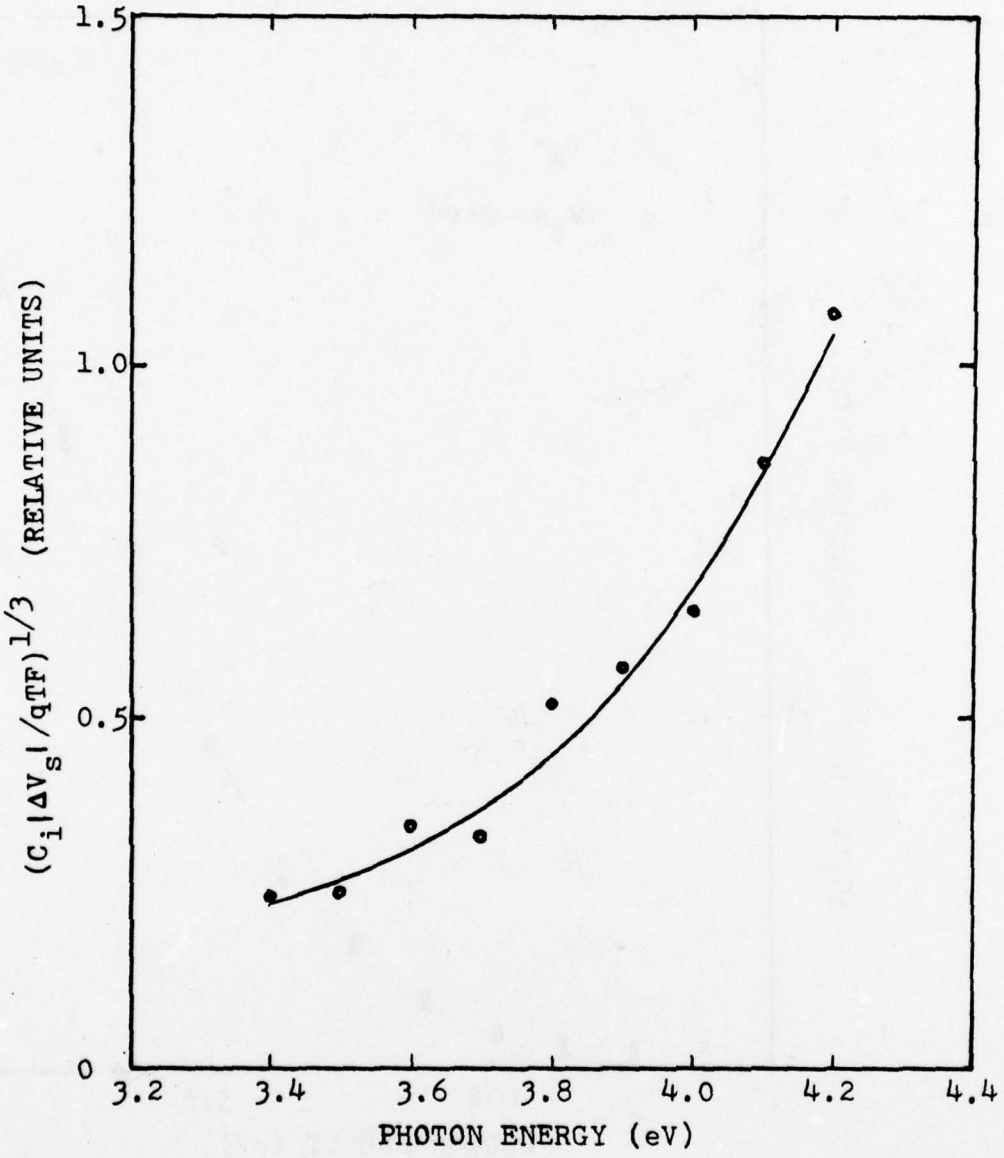

Fig. 4.2. $(C_i|\Delta V_s|/qTF)^{1/3}$ vs. photon energy for the sample having 1950Å Si_3N_4 and ~ 20Å on Si. A surface potential of 8V was used.

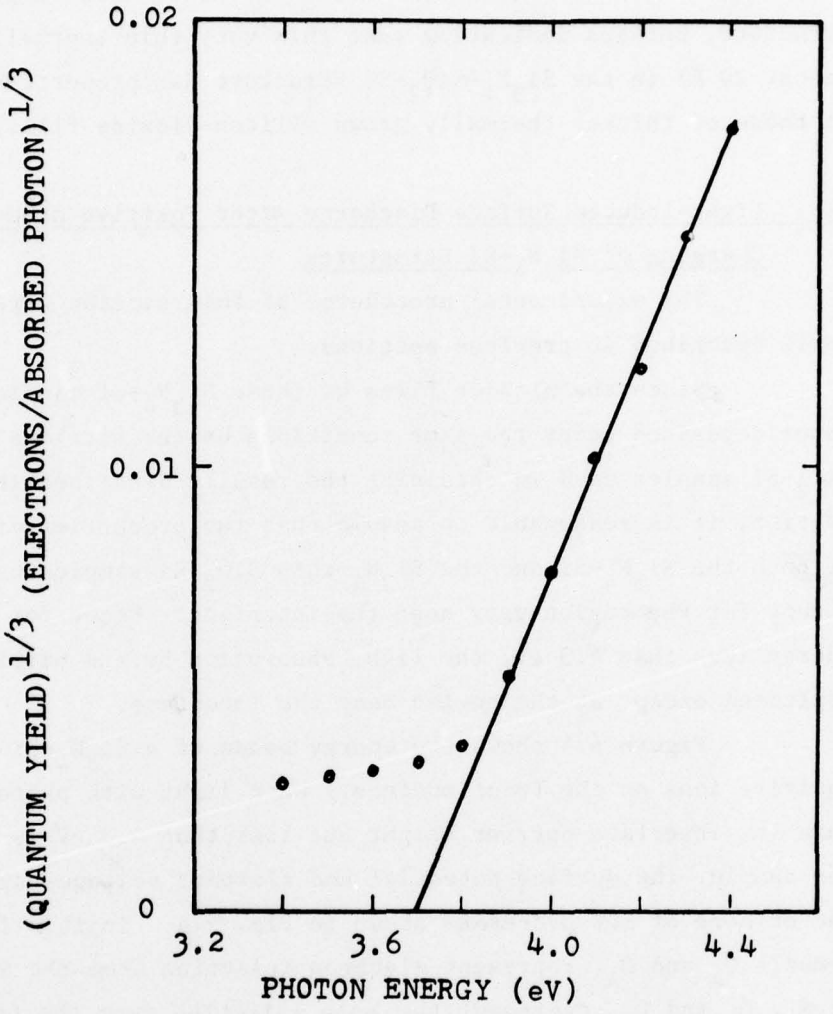

Fig. 4.3. (Quantum yield)$^{1/3}$ vs. photon energy for electron injection into a sample having 1950Å Si_3N_4 and $\sim$ 20Å SiO_2 on Si. A surface potential of 8V was used.

density of fixed surface charge (Q_{ss}).

Both the electron and hole internal-photoinjection properties of this structure are similar to those of the thermally grown SiO_2-Si structure, perhaps indicating that this very thin thermally grown oxide (about 20 Å) in the Si_3N_4-SiO_2-Si structure has properties very similar to those of thicker thermally grown silicon-dioxide films.

4.4. Light-Induced Surface Discharge after Positive or Negative Surface Charging of Si_3N_4-Si Structures

The experimental procedures of this section were the same as those described in previous sections.

Since the nitride films of these Si_3N_4-Si samples were chemically vapor deposited under the same conditions as the nitrides of the Si_3N_4-thin SiO_2-Si samples used in obtaining the results described in the previous section, it is reasonable to assume that the properties of the nitrides of both the Si_3N_4-Si and the Si_3N_4-thin SiO_2-Si samples were the same except for the region very near the interface. Hence for light with photon energy less than 4.3 eV, the light absorption by the nitride can be neglected except at the region near the interface.

Figure 4.4 shows the energy bands of a Si_3N_4-Si structure having positive ions on the front surface. When light with photon energy larger than the interface barrier height but less than 4.3 eV is incident on the sample, the surface potential and flatband voltage can change through one or more of the processes shown in Fig. 4.4. In this figure, the symbols Q_A and $Q_{A'}$ represent electron injection from the Si into the Si_3N_4, Q_D and $Q_{D'}$ represent the hole injection from the front surface into the nitride, Q_B represents the excitation of a hole from a localized state which is located very near the interface (and we assume that it is near enough to the interface that the hole can reach the substrate), Q_c represents hole-electron pair production by excitation across the bandgap at a position very near the interface (and we assume that it is near enough to the interface that the hole can reach the substrate), and X_A, X_B, X_C, X_D are the locations of the centroids of the charges created in the nitride by processes A, B, C. D respectively. We can write the following relations:

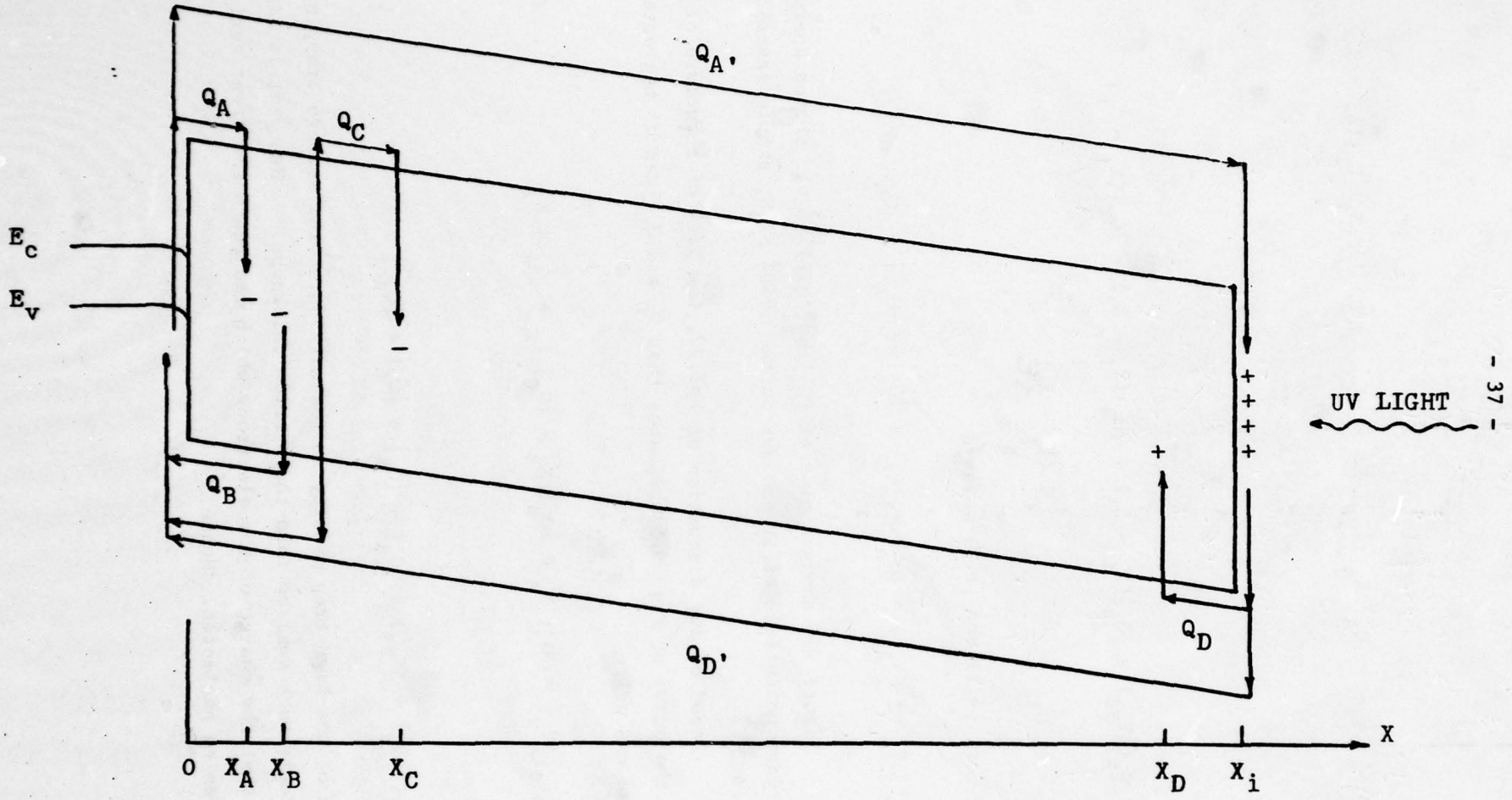

Fig. 4.4. Band structure of a nitride-on-silicon structure with positive ions on the front surface, and the possible mechanisms of light-induced changes in surface potential and flatband voltage.

$$X_i C_i |\Delta V_s| \simeq |Q_A| X_A + |Q_B| X_B + |Q_C| X_C + |Q_A,| X_i + |Q_D| (X_i - X_D) + |Q_D,| X_i \quad (4.1)$$

and

$$X_i C_i (\Delta V_{FB}) \simeq |Q_A| (X_i - X_A) + |Q_B| (X_i - X_B) + |Q_C| (X_i - X_c) - |Q_D| (X_i - X_D) \quad (4.2)$$

Adding Eqs. (4.1) and (4.2) we have

$$C_i (|\Delta V_s| + \Delta V_{FB}) \simeq |Q_A| + |Q_B| + |Q_C| + |Q_A,| + |Q_D,|$$

Figure 4.5 shows a plot of $(C_i |\Delta V_s| / qTF)^{1/3}$ vs. photon energy for surface potentials of 9V and -9V on the 1950Å Si_3N_4 sample described in Sec. 4.2.

Based on the discussion of Ref.17, the lack of structure of R/T in the curve of Fig. 4.5 indicates that Q_D and Q_D, can be neglected. Hence we can write

$$X_i C_i |\Delta V_s| \simeq |Q_A| X_A + |Q_B| X_B + |Q_C| X_C + |Q_A,| X_i \quad (4.3a)$$

and

$$C_i (|\Delta V_s| + \Delta V_{FB}) \simeq |Q_A| + |Q_B| + |Q_C| + |Q_A,| \quad (4.3b)$$

Because of the high trap density in the nitride,[34] the average trapping distance is much smaller than the nitride thickness. Hence it is highly likely that the charge of the electrons which can reach the front surface (Q_A,) can be neglected. Hence

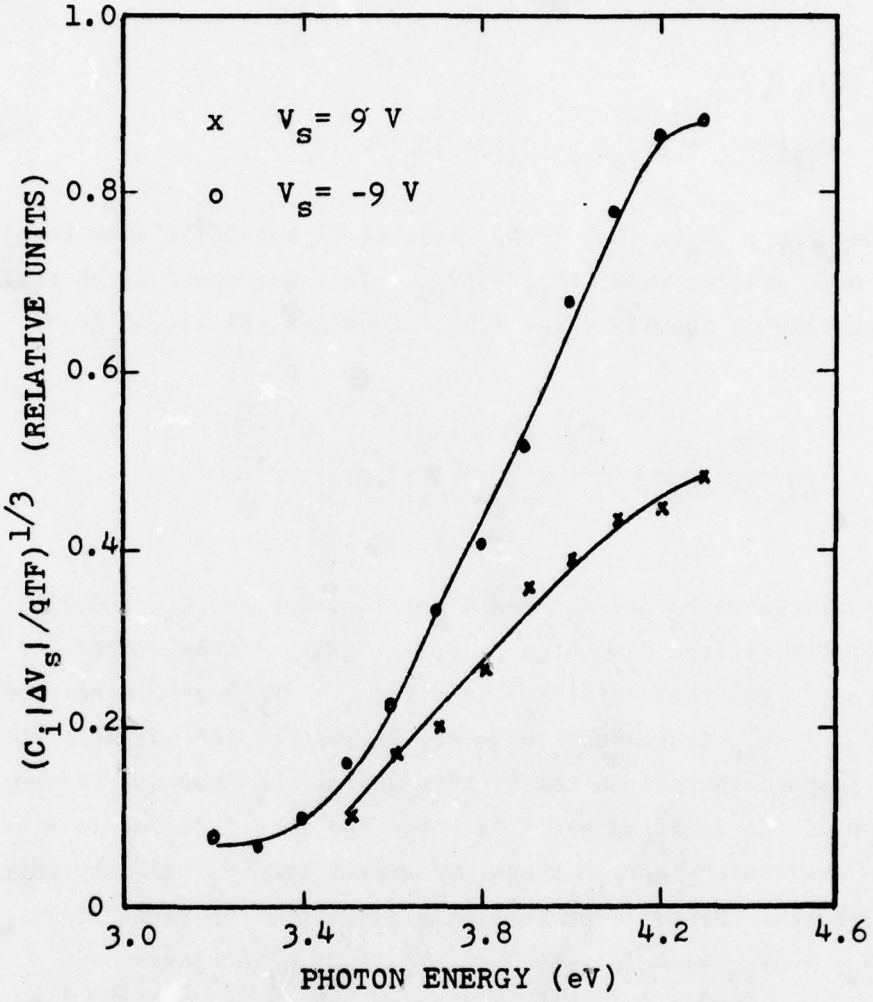

Fig. 4.5. $(C_i|\Delta V_s|/qTF)^{1/3}$ vs. photon energy for two surface potentials, +9 and -9V, for the structure having 1950Å Si_3N_4 on Si (see Sec.4.2).

$$X_i C_i |\Delta V_s| \simeq |Q_A| X_A + |Q_B| X_B + |Q_C| X_C \tag{4.4}$$

and

$$C_i(|\Delta V_s| + \Delta V_{FB}) \simeq |Q_A| + |Q_B| + |Q_C| \tag{4.5}$$

Since $|X_A|$, $|X_B|$, $|X_C| \ll X_i$, Eqs. (4.4) and (4.5) show that $|\Delta V_s|$ should be much smaller than $|\Delta V_s| + \Delta V_{FB}$. This was found to be true in the experimental results (Fig. 4.6). From Eqs. (4.4) and (4.5),

$$\frac{|\Delta V_s|}{|\Delta V_s| + \Delta V_{FB}} \simeq \frac{|Q_A| \frac{X_A}{X_i} + |Q_B| \frac{X_B}{X_i} + |Q_C| \frac{X_C}{X_i}}{|Q_A| + |Q_B| + |Q_C|} \tag{4.6}$$

The distances X_A and X_B should not increase as $|Q_B|$ and $|Q_C|$ increase. Therefore if the discharge is dominated by either or both of the processes B and C, the ratio of $|\Delta V_s|$ to $(|\Delta V_s| + \Delta V_{FB})$ should not increase as $|\Delta V_s| + \Delta V_{FB}$ increases. However, because of the possible photodepopulation of trapped charges in the nitride and/or the increase of the mean free path of the injected electrons near the interface due to a decrease in the available electron traps, we expect that X_A will increase as $|Q_A|$ increases. Hence if process A is dominant, the ratio of $|\Delta V_s|$ to $|\Delta V_s| + \Delta V_{FB}$ will increase as $|\Delta V_s| + \Delta V_{FB}$ increases.

Figure 4.6 shows a plot of $|\Delta V_s|/(|\Delta V_s| + \Delta V_{FB})$ vs $(|\Delta V_s| + \Delta V_{FB})$ for a surface potential of 10 V and $|\Delta V_s|/(|\Delta V_s| - \Delta V_{FB})$ vs. $(|\Delta V_s| - \Delta V_{FB})$ plot for a surface potential of -8.5 V. Light with a photon energy of 3.8 eV was used to discharge the samples. The substantial increase in the ratio as $|\Delta V_s| + \Delta V_{FB}$ increases indicates that process A is the dominant one under this experimental condition. That is, under our experimental conditions

$$|\Delta V_s| + \Delta V_{FB} \simeq |Q_A|/C_i \tag{4.7}$$

and

$$|\Delta V_s| \simeq |Q_A| X_A/C_i X_i \tag{4.8}$$

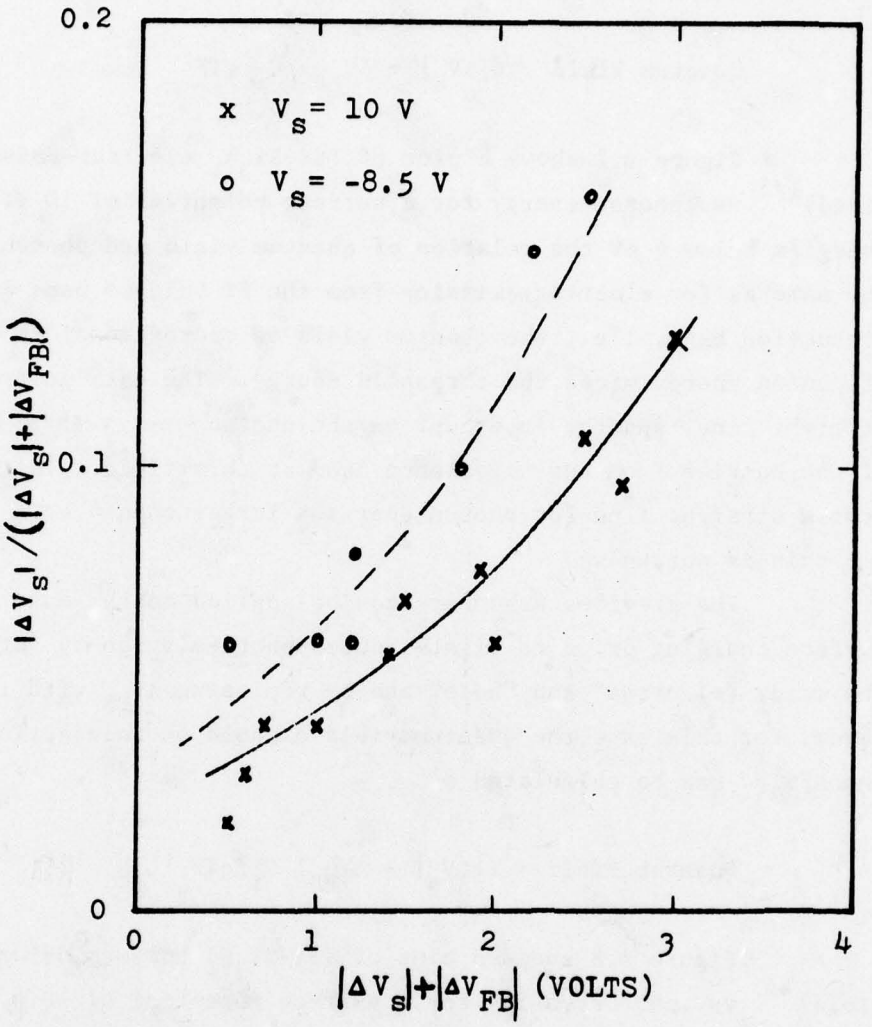

Fig. 4.6. $|\Delta V_s|/(|\Delta V_s| + \Delta V_{FB})$ vs. $(|\Delta V_s| + \Delta V_{FB})$ for surface potential 10V and $|\Delta V_s|/(|\Delta V_s| - \Delta V_{FB})$ vs. $(|\Delta V_s| - \Delta V_{FB})$ for surface potential of -8.5 V. The samples had 1950Å of Si_3N_4 on Si (see Sec. 4.2). Light with a photon energy of 3.8 eV was used to discharge the samples.

and the quantum yield for electron injection from Si into Si_3N_4 can be calculated as

$$\text{Quantum Yield} \simeq (|\Delta V_s| + \Delta V_{FB})\ C_i/qTF \tag{4.9}$$

Figure 4.7 shows a plot of (Si-Si_3N_4 electron-emission quantum yield)$^{1/3}$ vs. photon energy for a surface potential of 10 V. For photon energies below 4 eV the relation of quantum yield and photon energy is the same as for electron emission from the Si valence band into the SiO_2 conduction band, i.e., the quantum yield is proportional to the cube of photon energy minus the threshold energy. The data points follow a straight line, and the intercept on the photon-energy axis gives the height of the barrier from the Si valence band at this field. The data deviate from a straight line for photon energies larger than 4 eV. The reason for this is not known.

The previous arguments can be applied to the case of negative surface charging prior to light-induced photoemission by interchanging the words "electron" and "hole" and by replacing ΔV_{FB} with its negative. Hence, for this case the quantum yield of hole photoinjection from Si into Si_3N_4 can be calculated as

$$\text{Quantum Yield} \simeq (|\Delta V_s| - \Delta V_{FB})\ C_i/qTF \tag{4.10}$$

Figure 4.8 shows a plot of (Si-Si_3N_4 hole-emission quantum yield)$^{1/3}$ vs. photon energy for a surface potential of -8.5 V. The curve can be broken into two straight lines. This suggests the possibility of two injection processes. The intercepts of these two straight lines on the photon energy axis give the threshold energies of these two processes: 3.0 eV and 3.4 eV. The quantum yield of each process is proportional to the cube of the photon energy minus the threshold energy. The smaller threshold energy may correspond to the hole barrier energy from the Si conduction band at this field. The nature of the higher threshold energy is not known. An interesting point is that the hole injection quantum yield is larger than the electron injection quantum yield; for 3.5 to 4 eV photon, the hole photoinjection quantum yield is about 2.5 times larger than the electron photoinjection quantum yield.

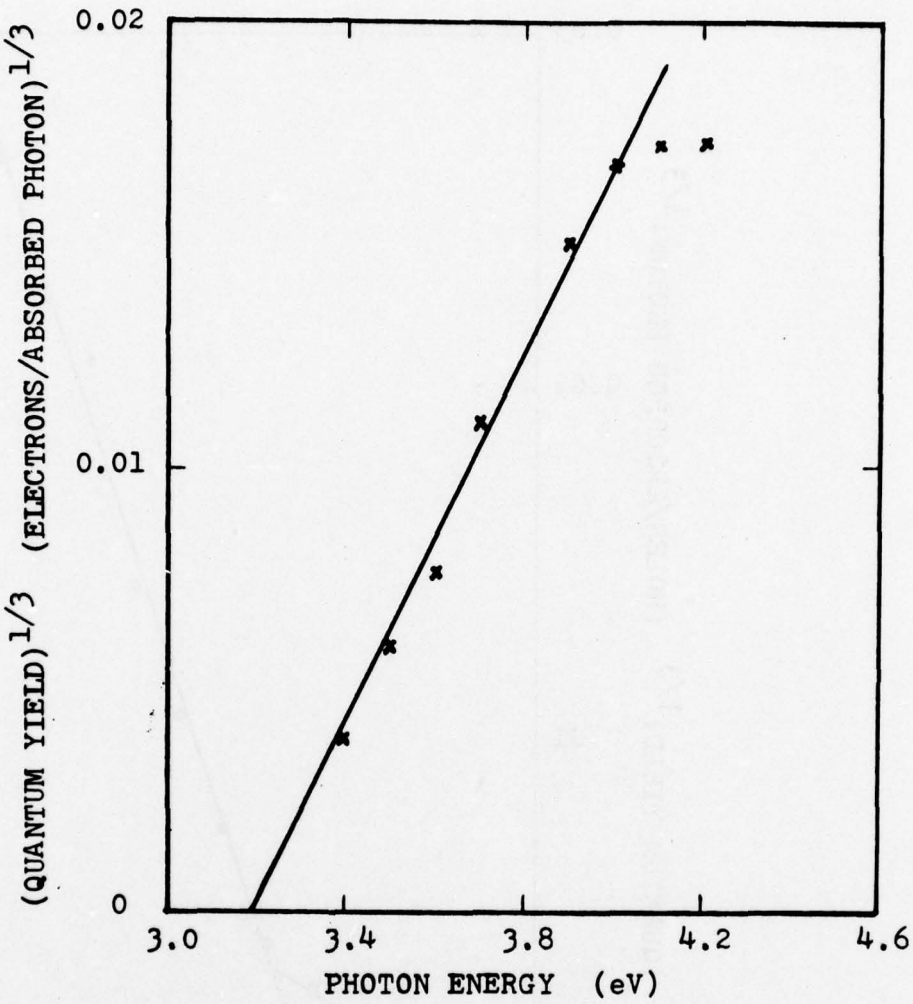

Fig. 4.7. (Si-Si_3N_4 quantum yield)$^{1/3}$ vs. photon energy for electron injection at surface potential of 10V. The sample had 1950 Å of Si_3N_4 on Si (see Sec. 4.2).

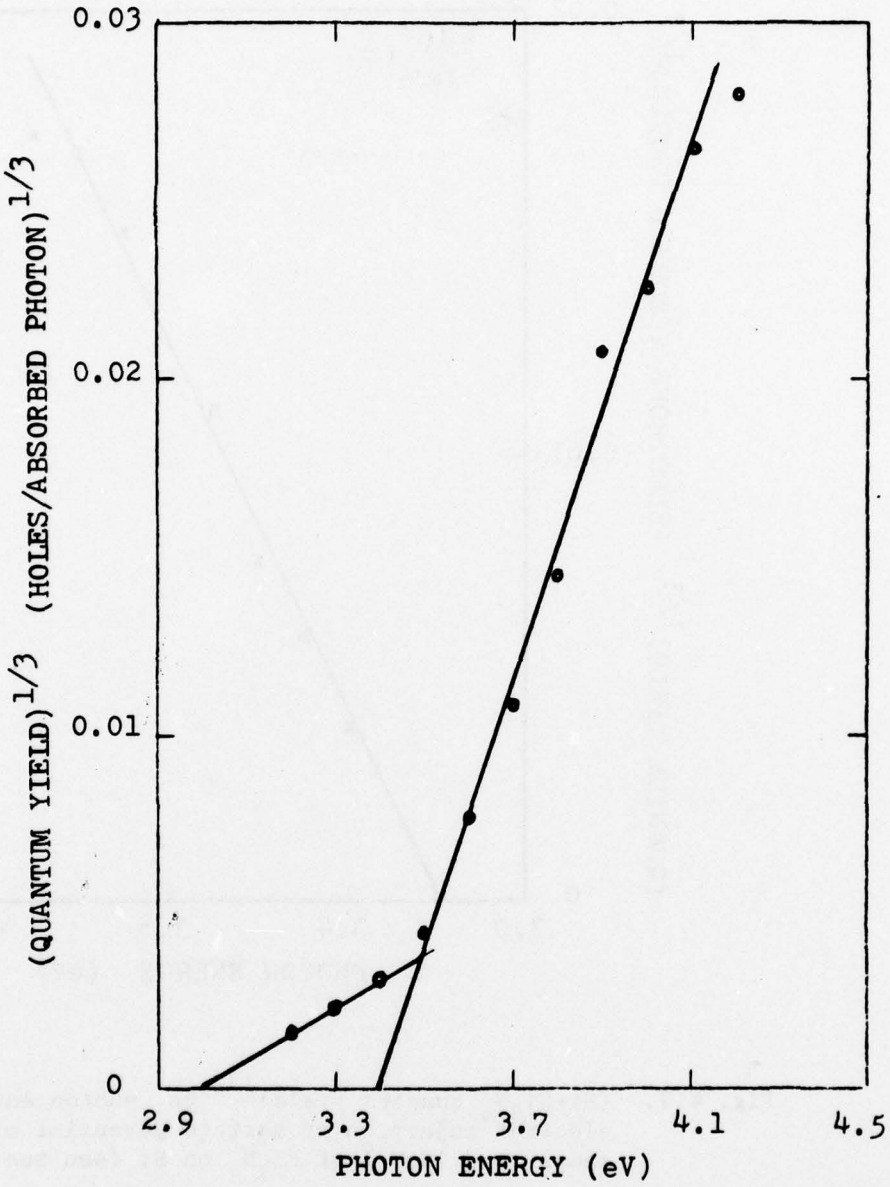

Fig. 4.8. (Si-Si_3N_4 quantum yield)$^{1/3}$ vs. photon-energy for hole injection at surface potential of -8.5V. The sample had 1950 Å of Si_3N_4 on Si (see Sec. 4.2).

The barrier height for zero field is difficult to estimate because of the lack of information about the distribution of charge in the nitride. However, we may make a zero-order estimate by assuming that the interface field is equal to the average nitride field and use the optical dielectric constant of the Si_3N_4 to calculate the Schottky barrier lowering. Then the zero-field electron(hole) barrier height from Si valence (conduction) band is found to be 3.4 eV (3.2 eV).

It has been believed that there is an unavoidable native oxide layer between the nitride and the silicon. The existence of this oxide layer was proved by P. H. Holloway and H. J. Stein,[30] using an ion probe. However, the results obtained in our work indicate that the properties of the native oxide must be quite different from those of thermally grown silicon dioxide.

4.5. Electron and Hole Traps in the Si_3N_4

The optical depths of the electron and hole traps in the nitride were studied by photodepopulation experiments, and the thermal depth of the electron and hole traps in the nitride were studied by thermal annealing experiments. The samples were 1950Å of Si_3N_4 on Si (see Sec. 4.2) and were annealed in forming gas (90% N_2, 10% H_2) at 500°C for 90 min.

4.5(A). Photodepopulation of Electron Traps

The electron traps in the nitride were filled by an internal photoemission of electrons from the Si substrate. Light with photon energies of 2 eV, 2.5 eV, and 3 eV was used to photo-depopulate the electron traps.

Typical experimental procedures and results are given in Table 4.1. After annealing in forming gas at 500°C for 90 min, the flatband voltages of the three samples, A, B, and C, were -4.4 V, -4.3V and -4.2V respectively. Sample A was the principal sample and samples B and C were the control samples. For samples A and B, process #2 and #3 (internal photoemission of electrons from the Si substrate into the nitride) were used to fill the electron traps in the nitride. After these steps, the ratio of $|\Delta V_s|$ to $|\Delta V_s| + \Delta V_{FB}$ was about 0.25. Since the average trapping

Table 4.1. Typical experimental procedures and results of the electron-trap photodepopulation experiments. The samples had 1950 Å of Si_3N_4 on Si (see Sec. 4.2). Sample A was the principal sample and samples B and C were the control samples. (X indicates process step did not occur.)

Process	V_{FB} (volts)*		
Sample:	A	B	C
1. Annealed in forming gas at 500°C for 90 min	-4.4	-4.3	-4.2
2. Exposed to positive corona to bring the surface potential to 10 V	(V_{FB} NOT MEASURED)	-4.3	X
3. Irradiated by 3.8 eV light with the intensity of 0.4 mW/cm^2 for one hour	V_{FB} NOT MEASURED	1.1	X
4. Exposed to negative corona to bring the surface potential to -4.5 V	(V_{FB} NOT MEASURED)	(V_{FB} NOT MEASURED)	X
5. Exposed to negative corona to bring the surface potential to - 8 V	X	X	(V_{FB} NOT MEASURED)
6. After 24 hrs storage in dark	0.4	0.3	-4.2
7. Process #6 repeated	X	0.35	X
8. Irradiated by 2 eV light with the intensity of 1 mW/cm^2 for 4 hrs	-0.5	X	(V_{FB} NOT MEASURED)
9. Process #8 repeated	-0.5	X	-4.2
10. Irradiated by 2.5 eV light with the intensity of 1 mW/cm^2 for 4 hrs	-1.2	X	(V_{FB} NOT MEASURED)
11. Process #10 repeated	-1.4	X	-4.2
12. Irradiated by 3 eV light with the intensity of 1 mW/cm^2 for 4 hrs	-1.8	X	(V_{FB} NOT MEASURED)
13. Process #12 repeated	-1.7	X	-4.2

* The average of the flatband voltages at two different points was used.

distance is very small in the nitride,[34] we can assume that the charge of the electrons which can reach the front surface can be neglected. From Eqs. (4.7) and (4.8), we have

$$X_A/X_i = |\Delta V_s|/(|\Delta V_s| + \Delta V_{FB})$$

where X_A is the distance from the centroid of the trapped charge to the interface and X_i is the thickness of the nitride. That is, most of the electrons were trapped in the bulk of the nitride rather than at the interface. Because of the small average trapping distance in the nitride,[34] the trapped charge profile shown in Fig. 4.9 should be a good approximation. If we keep the surface potential positive during the photodepopulation, any electron which was photoexcited to the nitride conduction band from electron traps located between the interface and X_t will drift toward the front surface and will be trapped between X_t and the front surface. The optical depth of the retrapped electrons may be larger than the photon energy of the light which was used for the photodepopulation, and this creates a problem. Hence, process #4 was used to charge the surface potential to -4.5 V by exposure to negative corona. Following this, storage in a dark and dry container for 24 hrs (process #6) resulted in reduction of flatband voltage, possibly due to charge emission from shallow traps at room temperature and/or the tunneling of trapped electrons very near the interface. After this step, the flatband voltage remained stable for at least an additional 24 hrs (process #7). Irradiation of the sample by 2 eV light with an intensity of about 1 mw/cm^2 for 4 hrs (process #8) reduced the flatband voltage to -0.5 V. Repeating this process resulted in little change of the flatband voltage, indicating that all the electron traps with depths less than 2 eV from the conduction band of the nitride had been photodepopulated. This result shows that about 20% of the deep electron traps (excluding those traps that are shallow enough to emit at room temperature) have optical depths less than 2 eV. Irradiation of the sample by 2.5 eV light with an intensity about 1 mw/cm^2 for 8 hrs (processes #10 and #11) reduced the flatband voltage to -1.4 V. This result shows that about 20% of the deep electron traps have optical depths between 2 eV and 2.5 eV.

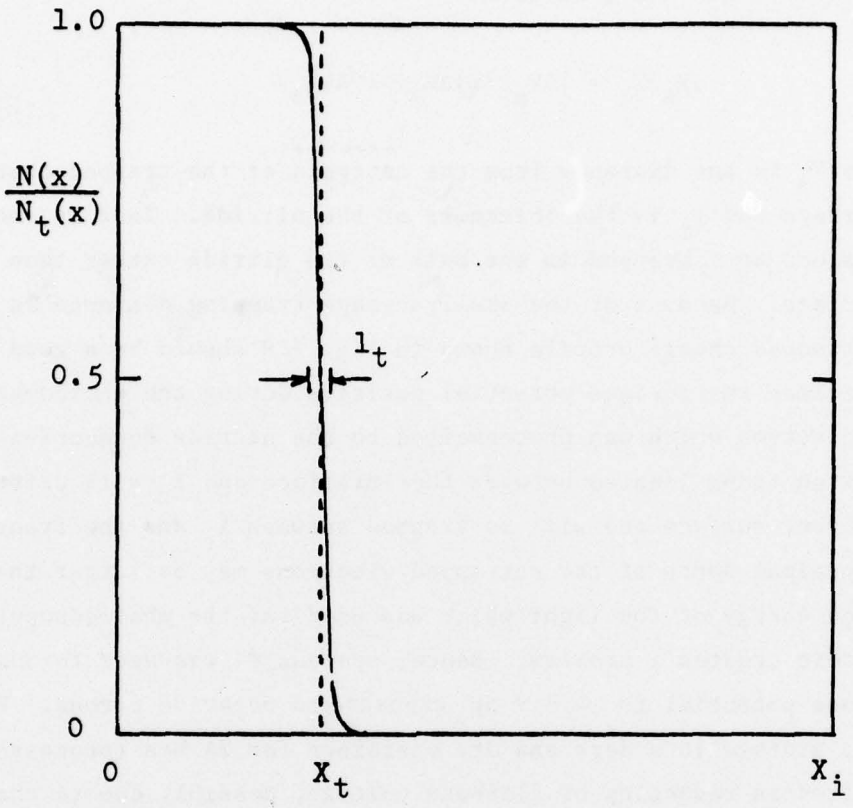

Fig. 4.9. Spatial charge distribution in the nitride. N(x) is the density of the trapped electrons (holes), $N_t(x)$ is the density of the electron (hole) traps, and ℓ_t is the average trapping distance. The origin of x is at the Si-Si_3N_4 interface. X_i is the thickness of the nitride. For a uniform N_t, the centroid of trapped charge is at $X_t/2$.

Irradiation of the sample by 3 eV light with an intensity about 1 mW/cm^2 for 4 hrs (process #12) reduced the flatband voltage to -1.8 V. Repeating this process resulted in a flatband voltage of -1.7 V. This small apparent increase of flatband voltage is probably due to experimental error caused by the nonuniformity of the flatband voltage over the surface of the sample. This result shows that about 8% of the deep electron traps have optical depths between 2.5 eV and 3 eV, and about 50% of the deep electron traps have optical depths greater than 3 eV.

In order to make sure that the flatband voltage shifts after the irradiation by light were caused by the photodepopulation rather than by charge injection, a control sample, Sample C, which had its electron traps unfilled, was charged to -8 V exposure to negative corona (process #5). This brought the interface field to a value approximately equal to that of the principal sample (Sample A) during processes #8 to #13. Then the sample was irradiated by light with photon energies of 2 eV (processes #8 and #9), 2.5 eV (processes #10 and #11), and 3 eV (processes #12 and #13), for 8 hrs each. No flatband voltage shift and no surface potential change were observed after these processes. Hence the changes of the flatband voltages of Sample A after these processes must have been due to the photodepopulation of the electron traps. We did not try using light with photon energy larger than 3 eV, because we knew from the results of the previous section that this would produce charge injection.

4.5(B). Photodepopulation of Hole Traps

The hole traps in the nitride were filled by internal photoemission of holes from the Si substrate into the nitride. Light with photon energies of 2 eV, 2.5 eV, and 3 eV was used to photodepopulate the hole traps.

Typical experimental procedures and results are given in Table 4.2. After annealing in forming gas at 500°C for 90 min, the flatband voltages of the three samples, A, B, and C, were -4.2 V, -4.3 V and -4.5 V respectively. Sample A was the principal sample and samples B and C were the control samples. For samples A and B, process #2 and #3 (internal photoemission of holes) were used to fill the hole traps in the nitride.

Table 4.2. Typical experimental procedures and results of the hole-trap photodepopulation experiments. The samples had 1950 Å of Si_3N_4 on Si (see Sec. 4.2). Sample A was the principal sample and samples B and C were the control samples. (X indicates process step did not occur.)

Process	Sample:	V_{FB} (volts)* A	B	C
1. Annealed in forming gas at 500°C for 90 min.		-4.2	-4.3	-4.5
2. Exposed to negative corona to bring the surface potential to -8 V		(V_{FB} NOT MEASURED)	-4.3	X
3. Irradiated by 3.8 eV light with the intensity of 0.4 mW/cm for one hr.		(V_{FB} NOT MEASURED)	-9.0	X
4. Exposed to positive corona to bring the surface potential to 3 V		(V_{FB} NOT MEASURED)	(V_{FB} NOT MEASURED)	X
5. Exposed to positive corona to bring the surface potential to 7.5 V		X	X	(V_{FB} NOT MEASURED)
6. After 24 hrs storage in dark		-8.2	-7.9	-4.5
7. Process #6 repeated		X	-7.95	X
8. Irradiated by 2 eV light with the intensity of 1 mW/cm for 4 hrs		-7.7	X	(V_{FB} NOT MEASURED)
9. Process #8 repeated		-7.6	X	-4.5
10. Irradiated by 2.5 eV light with the intensity of 1 mW/cm^2 for 4 hrs		-7.0	X	(V_{FB} NOT MEASURED)
11. Process #10 repeated		-7.0	X	-4.5
12. Irradiated by 3 eV light with the intensity of 1 mW/cm^2 for 4 hrs		-5.3	X	(V_{FB} NOT MEASURED)
13. Process #12 repeated		-5.2	X	-4.4

* The average of the flatband voltages at two different points was used.

After these steps, the ratio of $|\Delta V_s|$ to $|\Delta V_s| - \Delta V_{FB}$ was about 0.32. Since the average trapping distance is very small in the nitride, we can assume that the charge of holes which can reach the front surface can be neglected. Hence 0.32 X_i is the distance from the centroid of the trapped holes to the interface, where X_i is the nitride thickness. That is, most of the trapped holes were in the bulk of the nitride rather than at the interface. Because of the small average trapping distance in the nitride, the trapped charge profile shown in Fig. 4.9 should be a good approximation. If we keep the surface potential negative during the photodepopulation, any hole which was photoexcited from hole traps located between the interface and X_t will drift toward the front surface and will be trapped between X_t and the front surface. The optical depth of the retrapped holes may be larger than the photon energy of the light used for the photodepopulation, thus creating a problem. Hence process #4 was used to charge the surface potential to 3 V by exposure to negative corona. Following this, storage in a dark and dry container for 24 hrs (process #6) resulted in an increase of flatband voltage possibly due to a charge emission from shallow traps at room temperature and/or the tunneling of trapped holes very near the interface. After the foregoing step, the flatband voltage remained stable for at least an additional 24 hrs (process #7). Irradiation of the sample by 2 eV light with an intensity of about 1 mW/cm^2 for 4 hrs (process #8) increased the flatband voltage to -7.7 V. Repeating this process resulted in little change of the flatband voltage, indicating that all the hole traps with depths less than 2 eV from the valence band of the nitride had been photodepopulated. This result shows that about 15% of the deep hole traps (excluding those shallow traps that can emit their trapped holes at room temperature, have optical depths less than 2 eV. Irradiation of the sample by 2.5 eV light with an intensity of about 1 mW/cm^2 for 8 hrs (process #10 and #11) increased the flatband voltage to -7.0 V. This result shows that about 15% of the deep hole traps have optical depths between 2 eV and 2.5 eV. Irradiation of the sample by 3 eV light with an intensity of about 1 mW/cm^2 for 8 hrs increased the flatband voltage to -5.2 V. This result shows that about 45% of the deep hole traps have optical depths between 2.5 eV and 3 eV, and about 25% of the deep hole traps have optical depths greater than 3 eV.

In order to make sure that the flatband-voltage shifts after the irradiation were caused by photodepopulation rather than by charge injection, a control sample, Sample C, which had its hole traps unfilled, was charged to 7.5 V by exposure to positive corona (process #5). This brought the interface field of this sample to a value approximately equal to that of the principal sample (Sample A) during processes #8 to #13. Then the sample was irradiated by light with photon energies of 2 eV (processes #8 and #9), 2.5 eV (processes #10 and #11), and 3 eV (processes #12 and #13), for 8 hrs each. No flatband voltage shift and no surface-potential change were observed after these processes. Hence the changes of flatband voltage of Sample A after these processes must have been due to the photodepopulation of the hole traps. We did not try using light with photon energy larger than 3 eV because we know from the results of Sec. 4.4, that charge injection would then enter the picture.

4.5(C). Thermal Depth of the Electron and Hole Traps

It was found that trapped holes can be annealed out at 300°C for one hour in forming gas or nitrogen. The annealing of trapped electrons requires higher temperatures. The trapped electrons can be annealed out at 450°C for one hour in forming gas or nitrogen.

Arnett and Yun[34] found that the electron traps in the nitride are coulombic-attractive centers. Since there is no net charge in the nitride after annealing, we believe that the hole traps in the nitride are coulombic-attractive centers also. Hence it is reasonable to assume a capture cross section of the order of 10^{-13} cm^2. With this assumption, the thermal depths of the electron traps is calculated to be less than 2.6 eV and the thermal depths of the hole traps is indicated to be less than 1.7 eV. The thermal depths indicated here are much smaller than the optical depths.

4.6. Summary

In this chapter we have described our study of the light-induced surface discharge of Si_3N_4-Si and Si_3N_4-thin SiO_2-Si structures after positive and negative surface charging, together with a study of the electron and hole traps in the nitride.

The light-induced surface discharge of the Si_3N_4-thin SiO_2-Si system after positive surface charging for light with photon energy less than 4.3 eV was dominated by electron injection from the substrate. The injection properties were very similar to those of thick thermally-grown oxide except that the barrier height was about 0.27 eV smaller. No hole injection was observed in this system. These observations suggest that this very thin oxide ($\sim$ 20 Å) has properties similar to those of thick thermally-grown oxides.

It was found that the light-induced surface discharge of the Si_3N_4 system, using light with photon energy less than 4.3 eV, was dominated by electron injection from the substrate for positive surface charging and was dominated by hole injection from the substrate for negative surface charging. The injection quantum yield of either electrons or holes was proportional to the cube of the photon energy minus the threshold energy. The zero-field barrier height was found to be 3.4 eV for electron injection and 3.2 eV for hole injection. The electron and hole internal photoemission properties of this structure were quite different from those of thermally grown SiO_2-Si structures, indicating that the native oxide between the Si and Si_3N_4 has properties quite different from those of thermally grown silicon dioxide.

We find that the electron and hole traps of the nitride are distributed continuously in the band gap and that the electron traps are deeper than the hole traps. About 45% of the deep electron traps (excluding those shallow traps that can emit trapped electrons at room temperature) have optical depths larger than 3 eV. About 25% of the deep hole traps (excluding those shallow traps that can emit trapped holes at room temperature) have optical depths larger than 3 eV. The thermal depths appear to be less than 2.6 eV for electron traps and 1.7 eV for hole traps. These thermal depths are much smaller than the optical depths.

5. HIGH FIELD EFFECTS IN Al_2O_3 ON Si

(S. S. Li collaborating)

5.1. Introduction

In previous reports[1,2,17] we presented preliminary results on a study of high field effects in the metal-aluminum oxide-silicon system. Here we report on further results; in particular we provide additional evidence that trap-assisted tunneling is the major mechanism by which electrons are injected into the oxide, and we give the results of more extensive studies of the phenomenon of dielectric breakdown in Al_2O_3.

5.2. Description of the Samples

The MOS capacitors, which were fabricated at Bell Laboratories by courtesy of David Boulin, had 900°C pyrolytically grown Al_2O_3 on both n-type and p-type (100) silicon substrates having resistivities in the 4-6 Ω-cm range. Both gold gates and aluminum gates were evaporated on the surface of the oxide. The oxide thicknesses were in the range from 450Å to 1086Å. The semitransparent gold gates had a resistivity of 5Ω/□. The resistivity of the semitransparent aluminum gates ranged from 10 Ω/□ to 22 Ω/□. Some samples had thick (1000Å) aluminum gates.

5.3. Further Studies of the Electron Injection Mechanism in Al_2O_3

5.3(A). Introduction

Previously,[2] we reported our conjecture that owing to the high concentration of electron traps in the Al_2O_3, the injection of electrons into the oxide takes place principally by trap-assisted tunneling. In the present section we give further evidence to support this conclusion.

Since CVD Al_2O_3 has many traps, the flow of charge carriers will be accompanied by a build-up of space charge. Therefore, characterizing the injection current requires not only a measurement of the external current but also a determination of the charging rate. The latter can be determined from a measurement of the flatband voltage shift vs. time.

In the previous report[2] we presented evidence that the injection of electrons into Al_2O_3 was by tunneling and that there was a thermally activated component as well. In order to study the relation between the tunneling current and the interface field, we performed some experiments

at liquid nitrogen temperature so that the thermally activated current could be neglected.

5.3(B). Theory

For an MOS capacitor with charge carriers injected into the insulator from the substrate, the measured external current is given by the following equation

$$J_{ext} = J_{out}\ (x = d) + \frac{dD}{dT} \tag{5.1}$$

where $J_{out}\ (x = d)$ is the particle current which drifts through the gate-insulator interface and D is the electric displacement at that interface. The origin for x has been taken at the substrate-insulator interface, and the thickness of the insulator is d. If the substrate is kept in accumulation or inversion such that the rate of change of the surface potential, $d\psi_s/dt$, is very small, the displacement current dD/dt can be replaced by dQ/dt where Q is the total amount of charge (per unit area) stored in the insulator. The charging rate is equal to the trapping rate minus the detrapping rate. Thus

$$J_{ext} = J_{out}\ (x=d) + \frac{dQ}{dt} \tag{5.2}$$

Furthermore,

$$J_{ext} = J_{out}(x=d) + \frac{dQ_T}{dt}\ (1 - \bar{x}_T/d) \tag{5.3}$$

where dQ_T is the charge trapped in time dt with the centroid $\bar{x}_T$, and dQ_D is the detrapped charge with the centroid $\bar{x}_o$. Rearranging Eq. (5.3) we obtain

$$J_{out}(x=d) - \frac{dQ_D}{dt} + \frac{dQ_T}{dt} = J_{ext} + \frac{d}{dt}\ C_{ox}\Delta V_{FB} \tag{5.4}$$

Since $J_{out}(x=d)$ includes the detrapped charge carriers as well as the injected charge which flows all the way through the insulator, the

combination of the three terms on the left side of Eq. (5.4) gives the injection current. Hence:

$$J_{inj}(t) = J_{ext}(t) + \frac{d}{dt} C_{ox} \Delta V_{FB} \tag{5.5}$$

This result has been obtained previously, in a somewhat different way, by Arnett and DiMaria.[35]

The interface field is given by:

$$E(0) = (V_g - V_{FB} - \psi_s)/d - Q_{ss}^o /\varepsilon \tag{5.6}$$

where Q_{ss}^o is the surface-state charge at the flatband condition, ψ_s is the band bending at the silicon surface, and ε is the permittivity of the insulator.

5.3(C). Experiment

The samples used in this experiment had n-type substrates and Al_2O_3 with a thickness of about 450Å (see Sec. 5.2). The MOS samples were cooled down to 93°K. A C-V measurement carried out by sweeping from accumulation into weak depletion so that the flatband voltage could be obtained with minimal disturbance of the charge stored in the oxide. After the first C-V curve was taken, a constant voltage was applied to the capacitor. At various times, the current was recorded and the flatband voltage was also determined. It was observed that the time required for the sample to recover to its previous current level after each interruption was shorter at liquid nitrogen temperature than at room temperature. This again emphasizes the effect of temperature on the charge storage.

The amount of interface charge, Q_{ss}^o, was determined by the Gray-Brown method.[36] For one of our principal n-type samples, an increase of 5.4×10^{11} cm^{-2} in negatively charged surface states was observed after cooling to 93°K, whereas a check on a p-type sample showed a loss of 3.6×10^{11} cm^{-2} in negatively charged states. Since the surface states are primarily contributed by those peaks close to the band edges,[2] the change in the field could be approximated by using these measured

charge states. If all the charge states are acceptor like, the Q_{ss}^{o}/ε term in Eq. (5.6) will give the maximum field change to be 2×10^{5} V/cm. The ψ_s for our samples when operated in the accumulation region was calculated[37] to be $\sim$ 0.1 eV. Both terms were taken into consideration to correct the interface field strength.

5.3(D). Results

As shown in the previous report,[2] the external current at 93°K is observed to decay with time without reaching a steady state within an interval of 10^4 sec. Figure 5.1 shows the time dependence of flatband voltage for a typical sample. The initial fast charge build-up rate is ascribed to the large capture cross-section of the electron traps and the initially high injection current level. At low average field ($\sim$ 3 MV/cm) the current decays so fast that, above 300 seconds, no significant external current can be detected ($I \lesssim 10^{-13}$A), but a C-V flatband shift can still be measured. This indicates that the displacement current is very important at low fields.

By application of Eq. (5.5), we obtained the relation between the injected current at 93°K and the average insulator field at different times. This is shown in Fig. 5.2. The discrepancy between the injected current and the external current becomes more pronounced as the average oxide field decreases. Thus, at low fields, the injected carriers are mainly changing the charge storage within the oxide. In the moderate and high field range (E_{av} > 3.5 MV/cm), the displacement-current component decreases with time. There are probably two reasons for this: as time goes on, fewer traps are available, and furthermore the capture cross section of the traps at the leading edge of the trapping is reduced by the high field.

The interface field can be calculated with Eq. (5.6), using the measured values of V_g, V_{FB}, ψ_s and Q_{ss}^{o}. The results obtained for injected current at 93°K vs. interface field are plotted in Fig. 5.3. (It will be observed that the injection currents are much smaller at 93°K than they are at room temperature.[2,40,41]) The barrier height between the conduction band of the silicon substrate and the Al_2O_3 insulator has

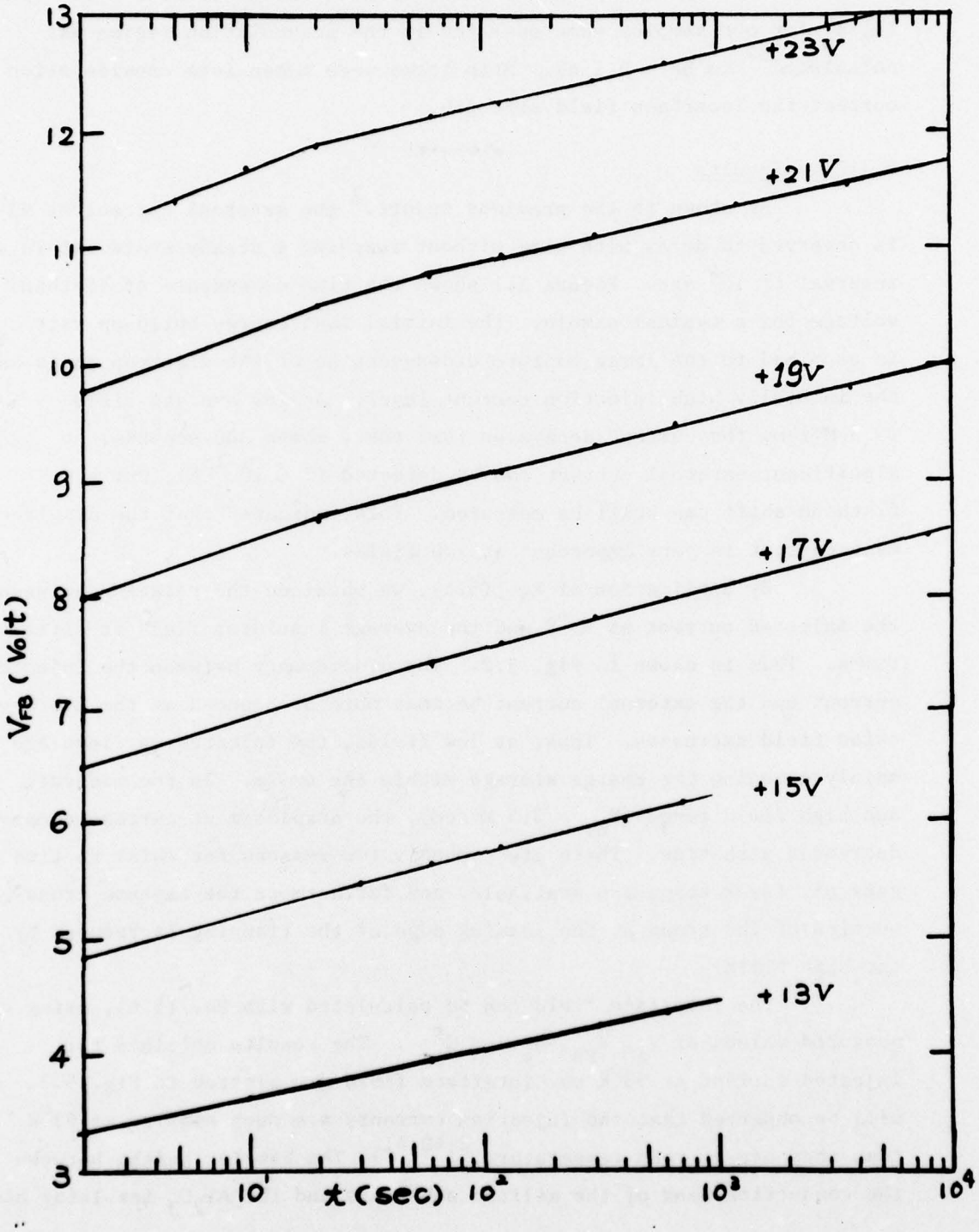

Fig. 5.1. Time dependence of flatband voltage for (n)Si-(450Å) Al_2O_3-Al structure for various applied voltages. The field stressing was done at 93°K.

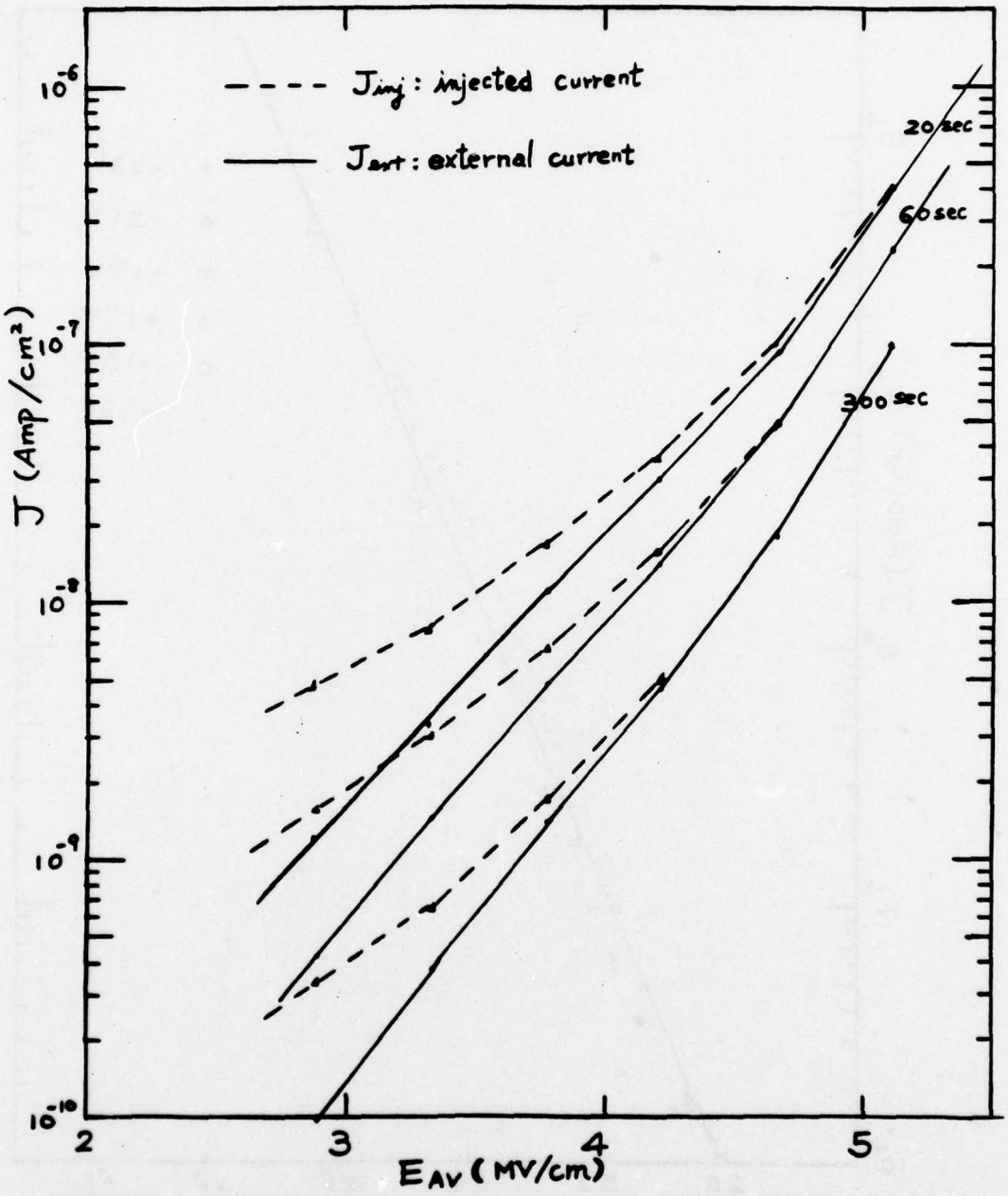

Fig. 5.2. The injected current and external current at 93°K vs. the average field in the insulator for a 450Å film of Al_2O_3, plotted for different times of stressing. The discrepancy between J_{inj} and J_{ext} is observed to be more pronounced at low fields. For moderate and high fields, the displacement current decreases with time.

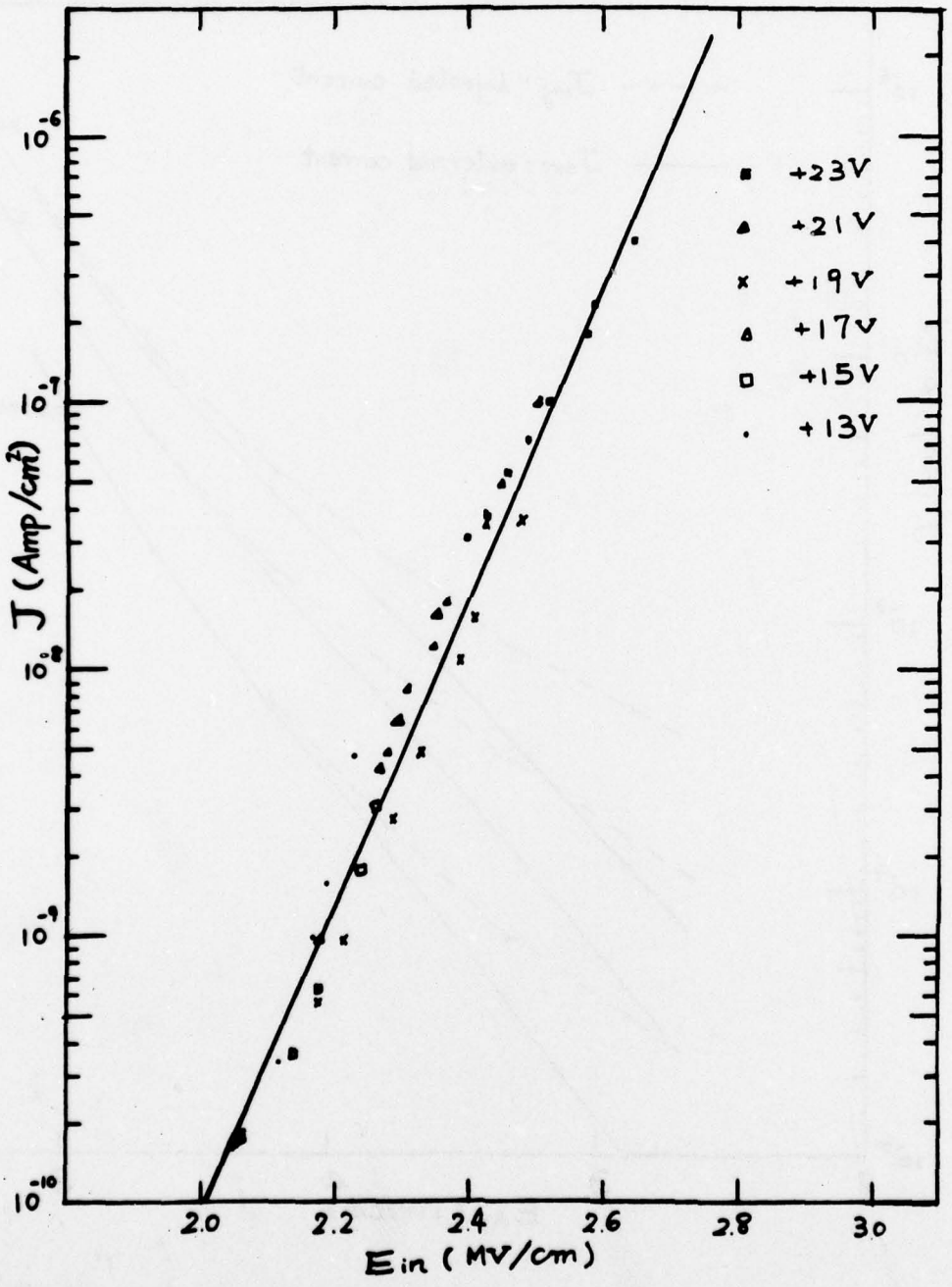

Fig. 5.3. The injected electron current at 93°K vs. the interface field. The data were obtained by stressing 6 MAS dots at voltages ranging from 13 V to 23 V.

studied by Szdlo and Poirier[38] and by DiMaria.[39] They find the barrier to be approximately 2.95 eV. If Fowler-Nordheim tunneling were the major mechanism responsible for the charge injection, the distance the charge carriers would have to travel to reach the conduction band of the oxide would be around 110Å, which seems very large. We have made a Fowler-Nordheim plot of the injection current vs. the interface field. Although the plot had good linearity, the slope gave the very low value of effective mass of 0.03 m_o. These two results make Fowler-Nordheim tunneling seem unlikely. However, due to the high concentration of the electron trapping close to the interface, a triangular barrier for the electrons to tunnel through can not be obtained and the conventional Fowler-Nordheim result does not apply. The negative space charge will change the barrier shape such that for the same interface field the current will be larger than when there is zero space charge. In order to calculate the tunneling probability for the electrons, the exact space charge distribution has to be known. Photodepopulation experiments have been done by Harari and Royce[42] and N. Johnson[43] to study the spatial distribution of the electron trapping. The trapping has been shown to be quite uniform throughout the bulk of the oxide. We analyzed the tunneling by considering two reasonable extreme cases. For the first of these we assumed that the space charge was uniformly distributed, and computed the minimum distance for the electrons to reach the Al_2O_3 conduction band to be approximately 100Å, and the maximum field to be 3.5 MV/cm. If Fowler-Nordheim tunneling were the major injection mechanism, then in order to satisfy the current level shown in Fig. 5.3, the effective mass would have to be somewhere in the range between 0.03 m_o - 0.09 m_o. For the other case, we assumed the space charge to be uniformly distributed from the oxide-substrate interface into the bulk to a depth of 116Å. Under this circumstance, the minimum tunneling distance was found to be approximately 80Å and the maximum field in the barrier was computed to be 4.5 MV/cm. The effective mass was between 0.03 m_o and 0.18 m_o. Thus, no matter what assumptions we made, the values we computed for Fowler-Nordheim tunneling did not seem reasonable.

We have previously found[3] the electron-trap concentration in our aluminum oxide to be very high: 2-3 x $10^{18}/cm^3$. In experiments to be described later, we found a significant amount of electron trapping to exist at optical depths less than 2.5 eV. As has been shown by O'Dwyer,[44] the presence of such traps in the tunneling barrier region will enhance the tunneling probability. The fact that a very high injection current can occur at relatively low fields and over relatively long distances suggests that trap-assisted tunneling is the important mechanism that we are observing.

From Fig. 5.3, an empirical relation between the injection current at 93°K and the interface field is found to be

$$J_{inj} = J_o \exp (E_{int}/E_o) \qquad (5.7)$$

where $E_o = 9.55 \times 10^4$ V/cm and $J_o = 2.68 \times 10^{-19}$ Amp/cm^2.
The injection current is extremely sensitive to the interface field. As the current continues to flow, the electron trapping process in the oxide continually reduces the interface field, and a steady-state current in the Al_2O_3 is very difficult to achieve.

5.4. Further Studies of Dielectric Breakdown in Al_2O_3

5.4(A). Introduction

Self-quenched breakdowns occur for both positive and negative bias in MAS capacitors with the gold gates.[2] Breakdown damage is also visible on Al gates after high field stressing. Hence we believe that breakdown is initiated from localized spots. It is observed that self-quenched breakdown events take place over quite a wide range of fields, and the breakdown frequency increases with the field strength. We have recorded the statistical results of the breakdown field for three different wafers. The strength of the insulator is observed to decrease as the temperature increases. If we bias an MAS capacitor near the critical breakdown field for a long period of time, a pre-breakdown current instability is observed in which the current fluctuates up and down. Once the instability has occurred, the sample can not

recover its stability, and even low field stressing will induce the instability and will eventually cause current runaway.

5.4(B). Breakdown Field for MAS Capacitors Under Positive Field Stressing

As has been shown previously,[2] the field strength of the Al_2O_3 insulator depends on the length of time that the stress is applied. In order to study the detailed breakdown process in a consistent way, each sample was biased for two hours at a field close to the critical field. If no breakdown occurred, the bias was increased by one volt and held again for two hours. This process was repeated until a breakdown occurred. The statistical results of the field strength obtained in this way for three different wafers are shown in Figs. 5.4, 5.5, and 5.6 for MAS capacitors with n-type substrates and 1000-Å Al field plates. The oxides for Figs. 5.4 and 5.5 were 450Å thick, and the oxide for Fig. 5.6 was 988Å thick. The figures show the cumulative percentage of broken-down capacitors, and the curves are continuous approximations to the discrete data. Curve 2 of Fig. 5.4 was taken at 93°K and shows the improved field strength obtained at that temperature over the room-temperature data shown by Curve 1. The data for Figs. 5.5 and 5.6 were taken at room temperature. The field at which 50% of the capacitors had broken down is noted on each curve. This field is 4.0, 4.4, and 4.0 MV/cm for wafers A, B, and C, respectively, at room temperature.

The discrepancy in the field strength between the two wafers A and B having the same oxide thickness shows the variability that can exist between samples that are apparently identical. In comparing the electronic properties of these two wafers, we found that the current level of Wafer A was an order of magnitude larger than that of Wafer B, although the C-V shifts were very similar for the two. Since the injection current level depends on the interface field as well as on the number of traps which can assist the tunneling process, we may conjecture that there may have been more shallow traps close to the interface in Wafer A. With regard to the improved field strength shown by Curve 2 of Fig. 5.4 at liquid nitrogen temperature, we take this to be strong evidence against impact ionization as the mechanism initiating breakdown.

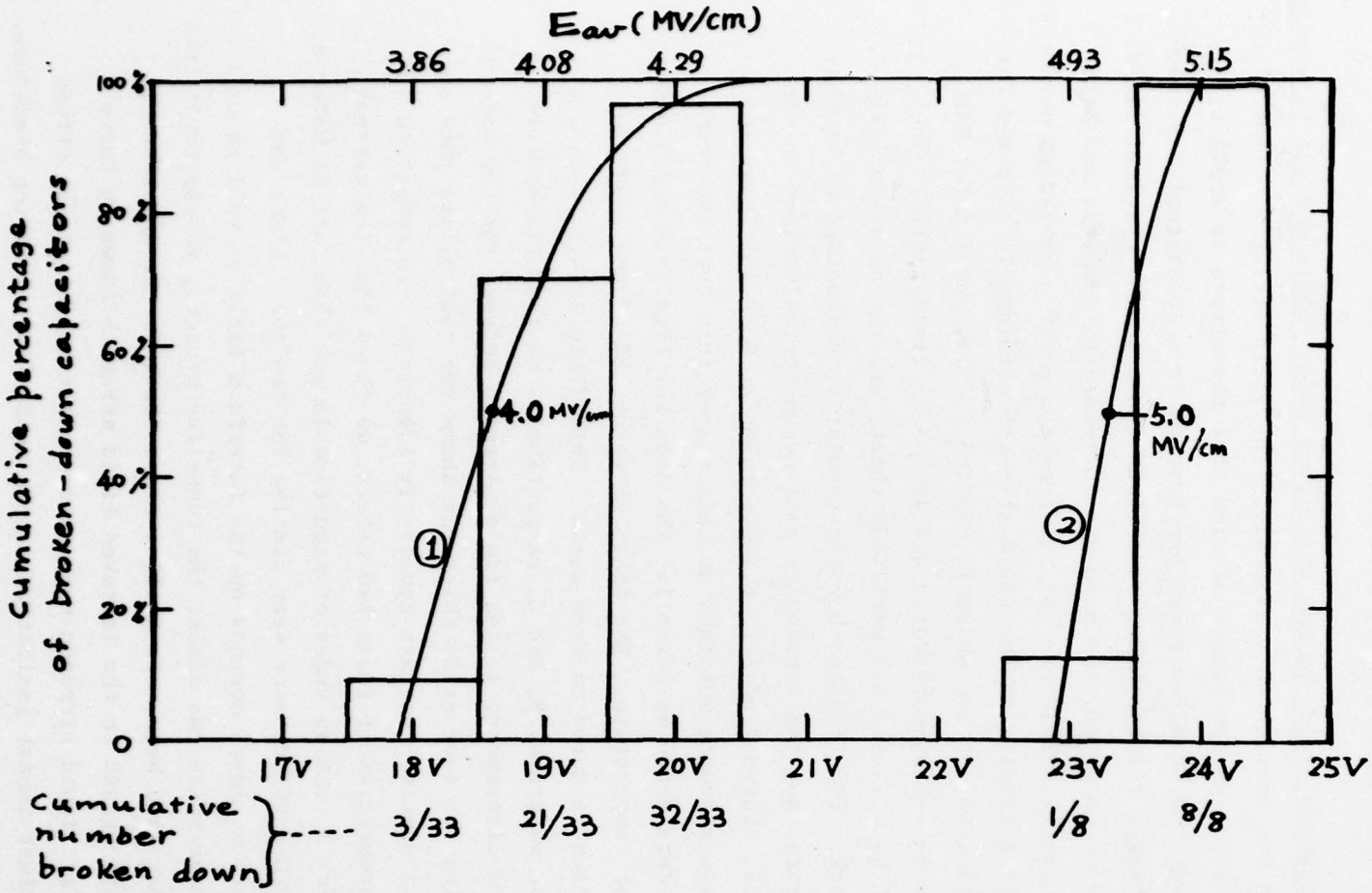

Fig. 5.4. Cumulative percentage of broken-down MAS capacitors vs. applied voltage for Wafer A. The voltage was incremented in 1-volt steps and each step was held for 2 hrs. Thickness of Al_2O_3: 450Å. The curves are continuous approximations to the discrete data. Curve 1: Data taken at room temperature. 33 capacitors were tested. Curve 2: Data taken at 93°K. 8 capacitors were tested.

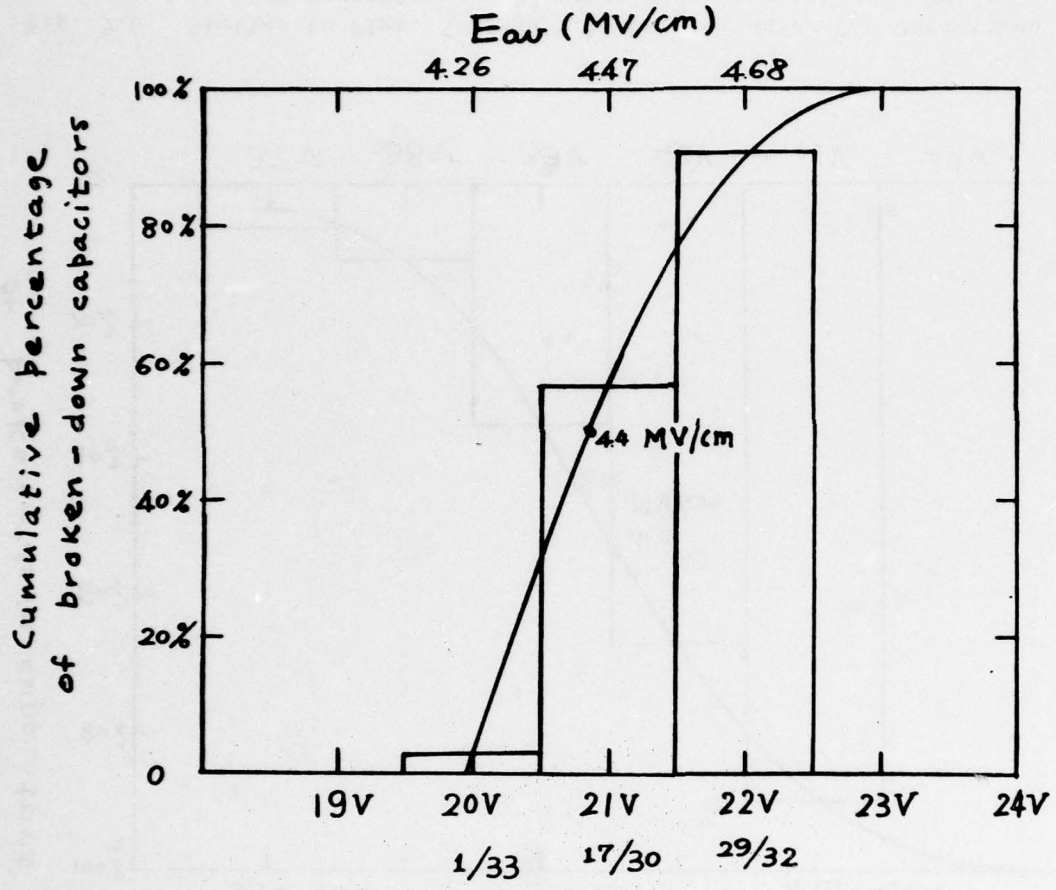

Fig. 5.5. Similar to Fig. 5.4, but for Wafer B. Data taken at room temperature only. 33 capacitors were tested. Oxide thickness: 450Å.

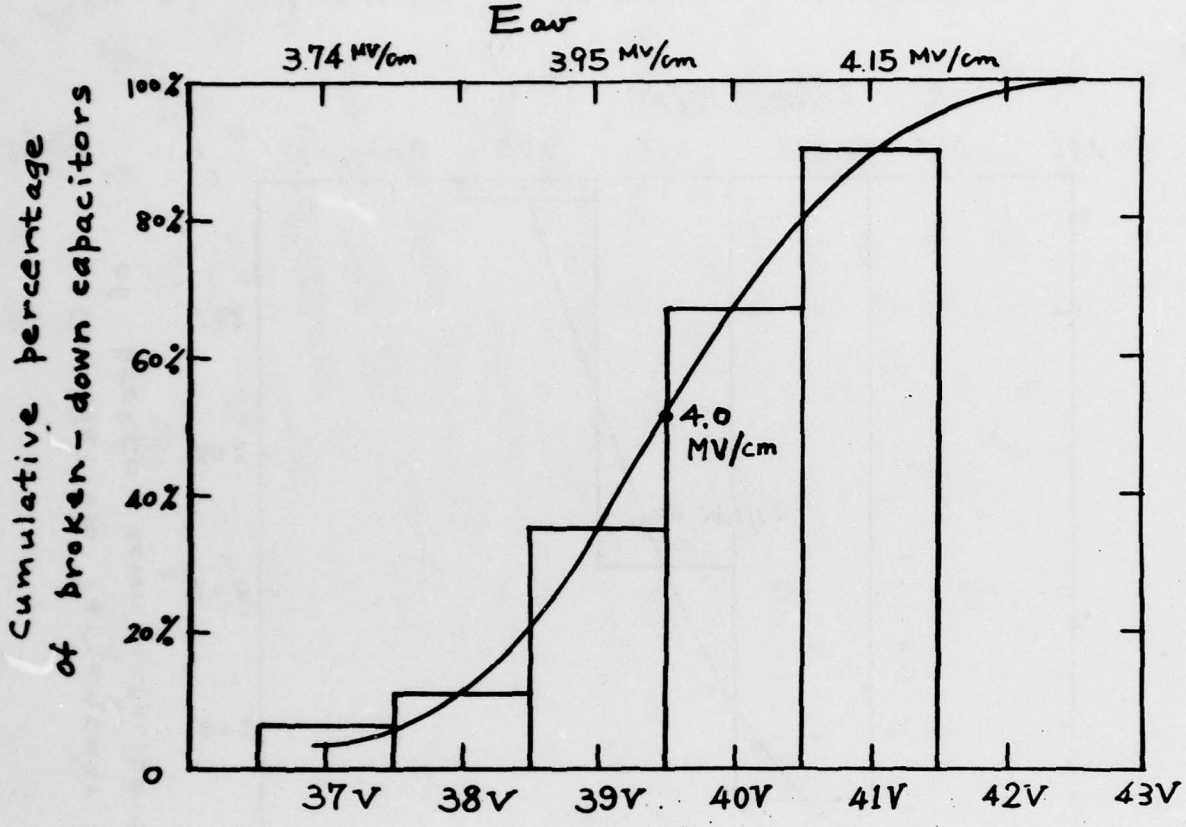

Fig. 5.6. Similar to Figs. 5.4 and 5.5, but for Wafer C. Data taken at room temperature. 27 capacitors were tested. Oxide thickness: 988Å.

We investigated the effect of temperature further, with the results shown in Fig. 5.7. Here we plot the current density vs. time at a particular applied voltage for three different temperatures, using capacitors from Wafer B. Higher temperature is seen to produce a larger current. In the experiment conducted at 122°C, three of the four capacitors used at that temperature broke down before the end of the run, one at 36 min, the second at 47 min, and the third at 63 min. The fourth capacitor broke down after an additional 44 min at 20 V. None of the samples tested at 25°C or 93°K broke down during the course of the experiment.

5.4(C). Self-Quenched Breakdowns

We have reported previously[2] that when an MAS capacitor with a gold field plate is subjected to high negative* field stressing, the self-quenching effect[6] is observed upon breakdown, and once the breakdowns start they continue to occur at an every-increasing rate until finally the sample reaches a condition of high conduction. The breakdown spots on the gate have been optically studied under the microscope and found to be of irregular shape no matter whether the silicon substrate is n-type or p-type.

The self-quenching effect also occurs in Au-Al_2O_3-Si MAS capacitors when they are stressed in high positive field. The samples we used were MAS capacitors with n-type substrates and an oxide thickness of 1089Å, and a second set having p-type substrates and an oxide thickness of 881Å. Each was biased at a field which should ultimately result in breakdown and was held at that field for two hours. The number of self-quenched breakdowns occurring in that time was noted. Then the field was increased and held for an hour, and the number of breakdowns was counted. The process was continued by increasing the field at one-hour intervals until the breakdown rate increased rapidly and the sample went into a high-conductance state. This generally occurred at a field strength in the neighborhood of 6.0-6.5 MV/cm. This is smaller than the limiting field strength found in corona-charging studies.[1] The large conductance

* The specification of "negative" or "positive" refers to the polarity of the field plate with respect to the substrate.

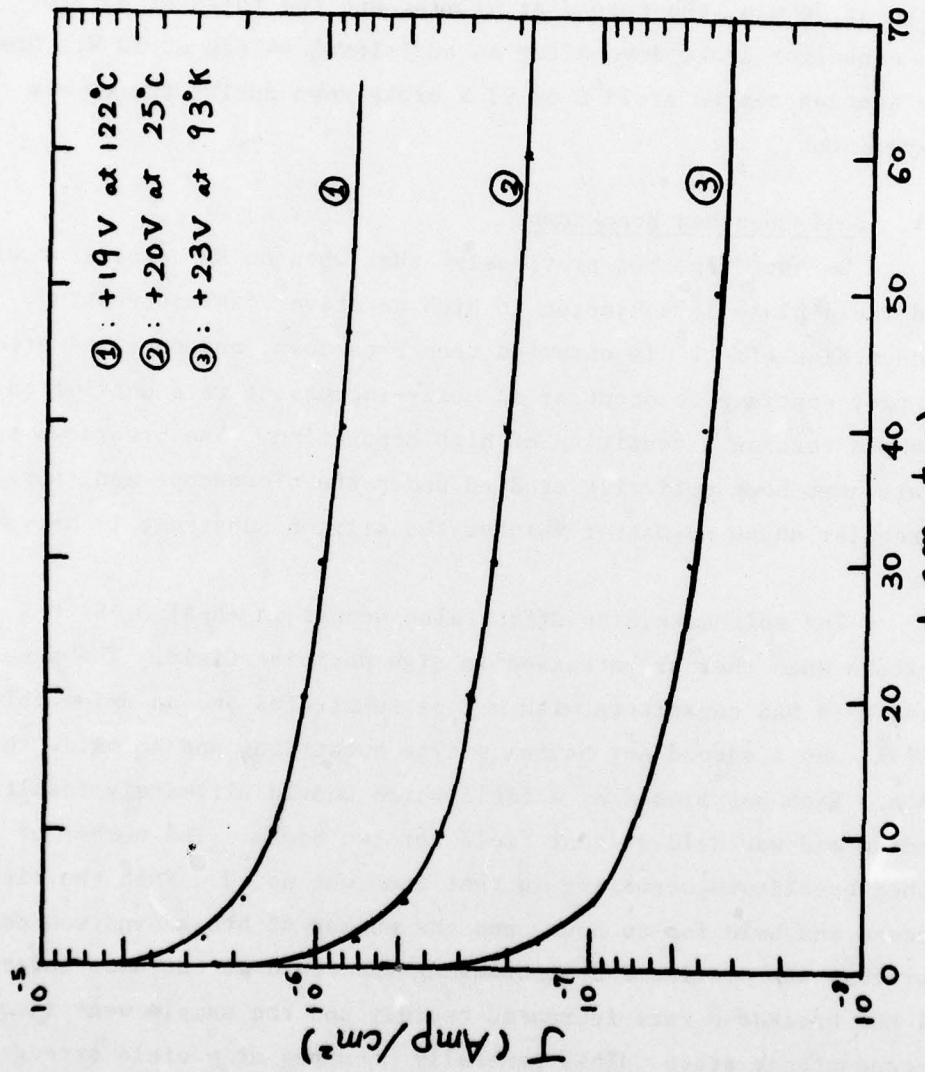

Fig. 5.7. Current vs. time for three particular voltages at three different temperatures. Oxide thickness: 450Å.

is probably caused by an incomplete self-quenched breakdown.

Optical micrographs of typical damage spots are shown in Fig. 5.8. With an n-type substrate and gold field plate biased positively, the breakdown spot is of circular shape with diameter around 7 μm, the exact size depending on the applied field. With a p-type substrate and gold field plate biased positively, the damage spot is observed to be much smaller even at relatively high fields, as shown in Fig. 5.8(b). During the course of the breakdown, a large impulse of current can be observed with an n-type sample, but only a small impulse of current is seen with the p-type sample. Close examination of the breakdown regions of the p-substrate sample shows a considerable amount of debris left on the perimeter of the breakdown spots. It appears that although the heat generated by the impulse current is sufficient to remove a portion of the gate, it is not sufficient to vaporize the debris. Because of the great amount of electron trapping in the oxide, the turn-on voltage for the inversion layer of the p-type substrate is very high. When breakdown occurs the surface potential of the substrate around the breakdown spot very quickly increases; thus the inversion layer around this spot is soon replaced by a depletion region. This severely limits the supply of free electrons and only a small impulse current is observed. For an n-substrate sample, electrons can be supplied both by the substrate and by the accumulation layer. Both the current and the temperature distribution around the breakdown spot have cylindrical symmetry. The high impulse current can generate enough heat to evaporate the gate. The evaporation occurs symmetrically around the center of the hole and produces a round breakdown spot.

With an aluminum field plate biased positively, no self-quenching effect was observed. The damage on an n-substrate sample with a 100Å Al field plate is shown in Fig. 5.8(c). A cluster of cracks appeared on the gate but no damage hole can be found.[2] The size of the cracked area depends on the field strength. Near the critical breakdown field, the cracked area is so small that we can determine the position of the original localized breakdown. Since the critical breakdown field is very nearly the same for both Au and Al under positive bias, it seems that the generated heat in the course of breakdown is able to take the gold gate

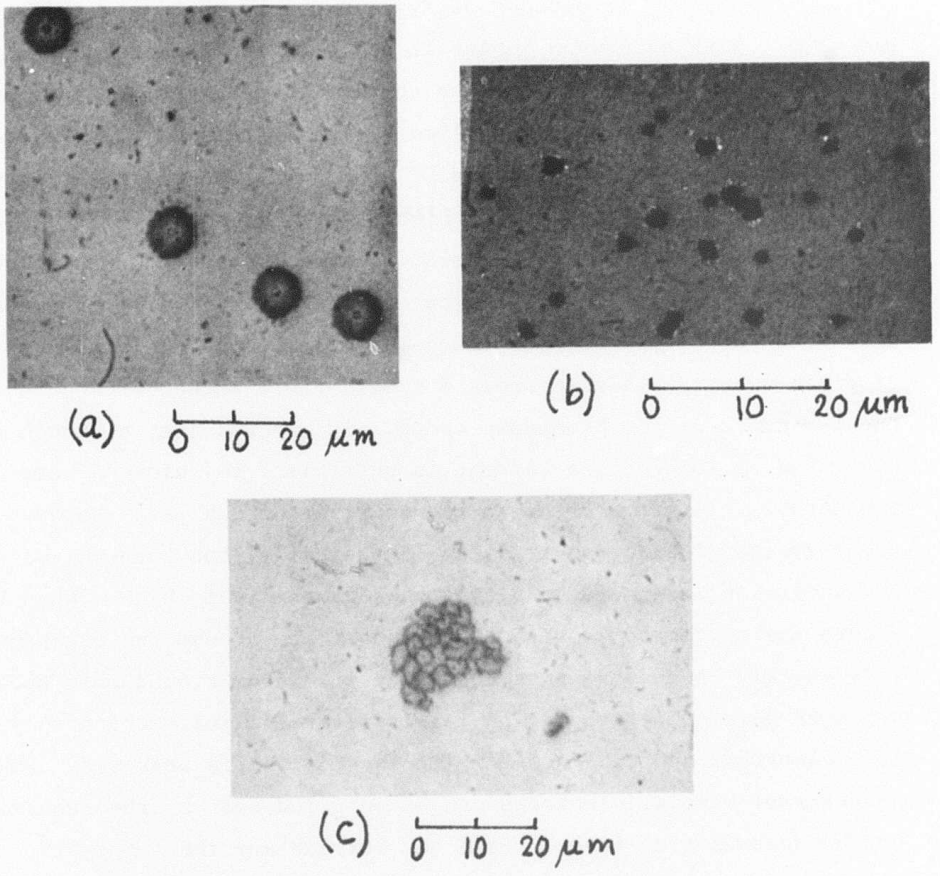

Fig. 5.8. Optical micrographs of self-quenched breakdowns.
(a) (100) n-Si/1089Å Al_2O_3/150Å Au. Biased at +60V.
(b) (100) p-Si/881Å Al_2O_3/150Å Au. Illuminated and biased at +56V.
(c) (100) n-Si/450Å Al_2O_3/100Å Al. Biased at +23V.

away but not the Al gate. The Al and Al_2O_3 interface may undergo a chemical reaction during the evaporation of the Al gate, resulting in a much stronger sticking force than between the Au and the Al_2O_3. If the pressure induced by the generated heat is not strong enough to overcome the sticking force, it may be dissipated through comparatively weaker lateral channels, producing branched cracks. We tried high field stressing on a somewhat thicker (200Å) Al gate, and found no damage spots on the field plate itself.

5.4(D). Pre-Breakdown Instability Initiated With Positive Applied Voltage

When an MAS sample is biased with the field plate positive at a constant voltage sufficiently high to cause ultimate breakdown, the current at first decreases smoothly and continuously until, at some time before breakdown, a current instability occurs. The instability consists of an increase in current, superimposed upon which is a set of rapid fluctuations. If the applied voltage is low enough that the time to breakdown is large, the duration of the pre-breakdown instability can be quite long, even as much as several hours in length. At higher voltages both the duration of the pre-breakdown instability and the time to breakdown are correspondingly short, and when the voltage is high enough to cause quick breakdown, the instability cannot always be seen but is presumably present nontheless. The instability is observed with both gold and aluminum field plates.

Once the instability has been initiated, the fluctuations in current persist even if the voltage is lowered, and they also continue to be seen if the polarity of applied voltage is reversed. After iniation of the instability, the voltage at which the insulator will break down is found to be lowered. An example of this behavior is shown in Fig. 5.9. This MAS sample had an n-type substrate, an oxide 450Å thick, and a 1000Å Al field plate. A voltage of +20.4V was applied to the fresh sample, and the current dropped steadily for about 42 min. A current instability then appeared, as is shown in Fig. 5.9(a). The applied voltage was then reduced to +15V, with the result shown in Fig. 5.9(b). Although the trend of the current is downward, substantial fluctuations persist. Figure 5.9(c) shows the result of reversing the bias and applying -17V. for 30 min. Fluctuations in the current are

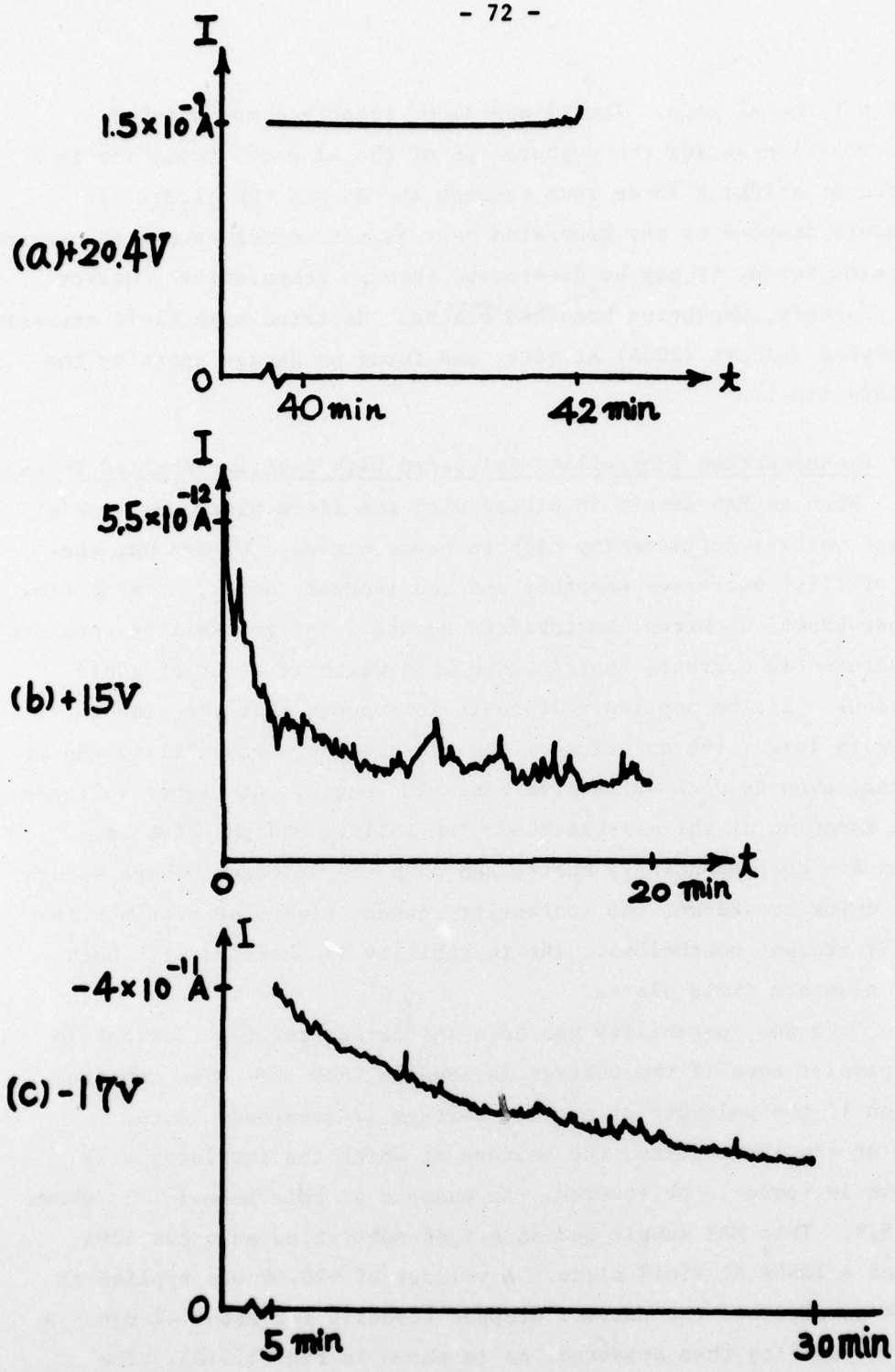

Fig. 5.9. Pre-breakdown current instability. n-Si/450Å Al_2O_3/1000Å Al.
(a) The instability appears after 45 min bias at + 20.4V.
(b) Bias reduced to + 15V for 30 min.
(c) Negative bias at -17V for 30 min.

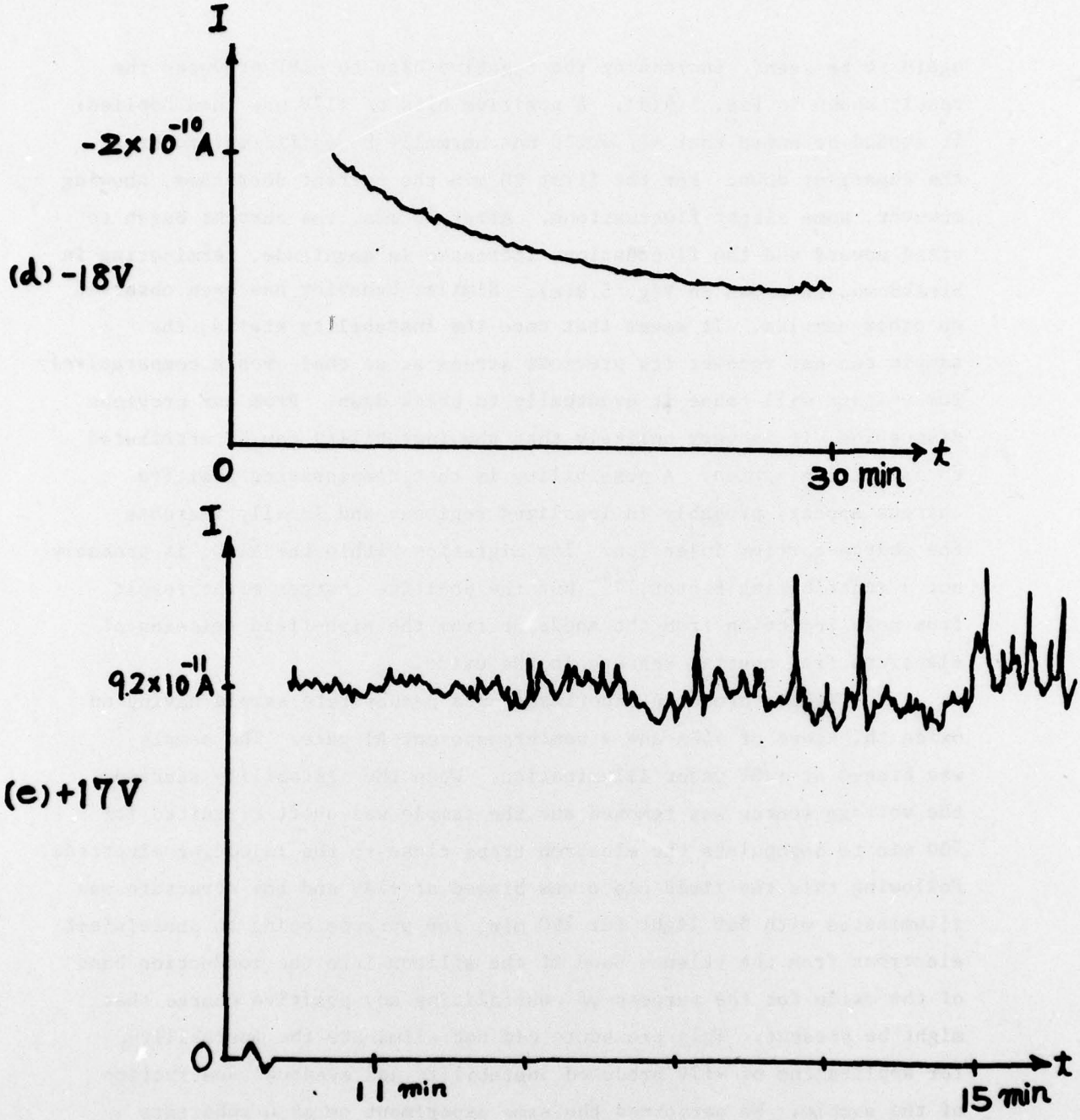

Fig. 5.9 (continued). (d) Negative bias at -18V for 30 min.

(e) Positive bias at +17V.
The instability becomes severe at ∿ 12 min
and breakdown finally ensued at 20 min.

again to be seen. Increasing the negative bias to -18V produces the result shown in Fig. 5.9(d). A positive bias of +17V was then applied. It should be noted that +17 would not normally be sufficient to break the capacitor down. For the first 10 min the current decreased, showing however, some slight fluctuations. After 10 min, the current began to trend upward and the fluctuations increased in magnitude, terminating in breakdown, as shown in Fig. 5.9(e). Similar behavior has been observed on other samples. It seems that once the instability starts, the sample can not recover its previous strength, so that even a comparatively low voltage will cause it eventually to break down. From our previous discussion, it is very unlikely that the instability can be attributed to impact ionization. A possibility is that compensating positive charges appear, probably in localized regions, and locally increase the charge-carrier injection. Ion migration within the Al_2O_3 is probably not a contributing factor,[2,42] but the positive charges might result from hole injection from the anode or from the high-field emission of electrons from neutral centers in the oxide.

We performed an experiment on a p-substrate sample having an oxide thickness of 450Å and a semitransparent Al gate. The sample was biased at +20V under illumination. When the instability started, the voltage source was removed and the sample was short circuited for 700 min to depopulate the electron traps close to the injecting electrode. Following this the field plate was biased at +14V and the structure was illuminated with 5eV light for 260 min, the purpose being to photoinject electrons from the valence band of the silicon into the conduction band of the oxide for the purpose of neutralizing any positive charge that might be present. This procedure did not eliminate the instability, for application of +17V produced instability and eventual destruction of the sample. We performed the same experiment on an n-substrate sample having an oxide thickness of 1089Å, and obtained a similar result, i.e., the photoinjection of electrons did not cure the instability.

The degradation of a sample can proceed very slowly. One n-substrate sample with a 450Å oxide was observed to have a decaying

current for 60 hours under 17 volt bias, after which the current started to increase and rose from 1.38×10^{-10} A to 1.6×10^{-10} A in the succeeding 10 hrs. Soon thereafter the sample burned out.

So far our investigations have been conducted principally with positive field-plate biasing, and we can propose at least two models to explain the high-field effects that we have observed. At the present time we are conducting a systematic investigation of the effects produced under negative field-plate bias. At the conclusion of the present study we hope to propose a model which satisfactorily explains the principal aspects of the observed high-field behavior.

REFERENCES

1. Walter C. Johnson, "Study of Electronic Transport and Breakdown in Thin Insulating Films," Semi-Annual Technical Report No. 3 (NVL-0059-005), Contract DAAG53-73-C-0059, 1 June 1977.

2. Walter C. Johnson, "Study of Electronic Transport and Breakdown in Thin Insulating Films," Semi-Annual Technical Report No. 4 (NVL-0059-007), Contract DAAG53-76-C-0059, 1 December 1977.

3. C. C. Chang, "Study of Lateral Nonuniformities and Interface States in MIS Structures," Ph.D. Dissertation, Department of Electrical Engineering, Princeton University, February 1976.

4. M. Kuhn, Solid State Electron., 13, 873 (1970).

5. C. S. Jenq and W. C. Johnson, "High-Field Generation of Interface States and Electron Traps in MOS Capacitors," Device Physics Laboratory Technical Report No. 35, Department of Electrical Engineering and Computer Science, Princeton University, Princeton, NJ 08540.

6. D. Y. Yang, W. C. Johnson, and M. A. Lampert, "A Study of the Dielectric Breakdown of SiO_2 Films on Si by the Self-Quenching Technique," Special Report No. 4 (AFCRL-TR-74-0516), October 1974.

7. T. W. Sigmon, W. K. Chu, E. Lugujjo, and J. W. Mayer, Appl. Phys. Lett., 24, 105 (1974).

8. R. Williams and A. M. Goodman, Appl. Phys. Lett., 25, 531 (1974).

9. R. Flitsch and S. I. Raider, J. Vac. Sci. Technol., 12, 305 (1975).

10. R. A. Clarke, R. L. Tapping, M. A. Hopper, and L. Young, J. Electrochem. Soc., 122, 1347 (1975).

11. W. L. Harrington, R. E. Honig, A. M. Goodman, R. Williams, Appl. Phys. Lett., 27, 644 (1975).

12. J. S. Johannessen, W. E. Spicer, and Y. E. Strausser, J. Appl. Phys., 47, 3028 (1976).

13. K. H. Zaininger, Appl. Phys. Lett. 8, 140 (1966).

14. C. C. Chang and Walter C. Johnson, IEEE Trans. Electron Devices ED-24, 1249 (1977).

15. Z. A. Weinberg, W. C. Johnson, and M. A. Lampert, J. Appl. Phys. 47, 248 (1976).

16. M. Lenzingler and E. H. Snow, J. Appl. Phys. 40, 278 (1969).

17. Walter C. Johnson, Semi-Annual Technical Report No. 1 (NVL-0059-001), Contract DAAG53-73-C-0059, 1 June 1976.

18. Walter C. Johnson, Semi-Annual Technical Report No. 2 (NVL-0059-003), Contract DAAG53-73-C-0059, 1 December 1976.

19. R. Williams and A. Willis, J. Appl. Phys. 39, 3731 (1968).

20. R. Williams and M. H. Woods, J. Appl. Phys. 44, 1026 (1973).

21. R. Williams, Phys. Rev. 140, A569 (1965).

22. Hu H. Chao and Wlater C. Johnson, "A Combined Corona and Photoemission Technique for Studying the Electronic Properties of Thin Insulating Films, With Application to Silicon Dioxide and Silicon Nitride," Device Physics Laboratory Technical Report No. 37, Department of Electrical Engineering and Computer Science, Princeton University, Princeton, NJ 08540, March 1978.

23. S. M. Hu, J. Electrochem. Soc., 113, 693 (1966).

24. T. L. Chu, C. H. Lee, and G. A. Gruber, J. Electrochem. Soc., 114, 717 (1967).

25. M. J. Grieco, F. L. Worthing, and B. Schwartz, J. Electrochem. Soc., 115, 525 (1968).

26. B. E. Deal, P. J. Fleming, and P. L. Castro, J. Electrochem. Soc., 115, 300 (1968).

27. V. Y. Doo, D. R. Kerr, and D. R. Nichols, J. Electrochem. Soc., 115, 61 (1968).

28. S. Zirinsky, J. Electro. Materials, 4, 591 (1975).

29. A. M. Goodman, E. C. Ross, and M. T. Duffy, RCA Review 31, 342 (1970).

30. P. H. Hollaway and H. J. Stein, J. Electrochem. Soc. 123, 723 (1976).

31. H. Maes and R. Van Overstraeten, Appl. Phys. Lett. 27, 282 (1975).

32. A. M. Goodman, Appl. Phys. Lett., 13, 275 (1968).

33. H. R. Philipp, J. Electrochem. Soc. 120, 295 (1973).

34. P. C. Arnett and B. H. Yun, Appl. Phys. Lett. 26, 94 (1975).

35. P. C. Arnett and D. J. MiMaria, J. Appl. Phys. 47, 5 (1976).

36. P. V. Gray and D. M. Brown, Appl. Phys. Letts. 8, 2, 31.

37. S. M. Sze, Physics of Semiconductor Devices, (Wiley, 1969), p. 430.

38. N. Szydlo and R. Poirier, J. Appl. Phys. 42, 4880 (1971).

39. D. J. DiMaria, J. Appl. Phys. 45, 5454 (1974).

40. R. H. Walden, J. Appl. Phys. 43, 1178 (1972).

41. R. J. Powell and G. W. Hughes, IEEE Trans. Nucl. Sci. NS-21, 179 (1974).

42. E. Harari and B. S. H. Royce, IEEE Trans. Nucl. Sci. NS-21, 280 (1973).

43. N. M. Johnson, Comments on "Trap Structure of Pyrolytic Al_2O_3 in MOS Capacitors", unpublished report.

44. J. J. O'Dwyer, The Theory of Electrical Conduction and Breakdown in Solid Dielectrics, (Clarendon Press, Oxford, 1973).